Exploring Full-Duplex Gains in Multi-Cell Wireless Networks: A Spatial Stochastic Framework

by

Shu Wang

Master Thesis submitted in partial fulfillment of
the requirements for the degree of

Master of Sciences

(Electrical and Computer Engineering)

at the

UNIVERSITY OF WISCONSIN–MADISON

2015

This thesis is dedicated to my family I love.

Acknowledgments

I am grateful to all the people who helped me during my master study at University of Wisconsin-Madison.

Foremost, I would like to express my sincere gratitude to my master supervisor, Professor Xinyu Zhang, for his continuous support during my Master study and research. I greatly benefited by his deep knowledge in wireless networks as well as novel research ideas. Without him, this thesis would not exist. Despite his knowledge, I am also deeply inspired by his enthusiasm and hardworking towards academic excellent. This spirit will encourage me to keep an optimistic attitude with hard work and perseverance, as I climb the "steep paths" during my future Ph.D study.

I am also sincerely grateful to my future Ph.D supervisor, Professor Shan Lu. I took her Operation System class when she was at University of Wisconsin-Madison, and really enjoyed her excellent class. She is patient and knowledgeable to answer my questions. After moved to the University of Chicago, she continued providing priceless suggestions and generous helps. I deeply appreciate her kindness, and try my best to contribute to her group.

Thanks also go to all members in the WiXNet research group. I want to thank Vignesh Venkateswaran for discussing the problems in our full-duplex stochastic geometry paper, and plotting the related figures. I also

want to thank Teng Wei for his help during our exciting acoustic-radio transformation projects. I gained lots of experience on Software Defined Radio, the knowledge on wireless networks as well as the way to do research. I want to thank Sanjib Sur for helping me present my first paper in INFOCOM 2015 and offering suggestions. I am also grateful to Xiufeng Xie, Jialiang Zhang, Chi Zhang, Tong Meng, Aditya Prakash and so on for making WiXNet a excellent research environment. By the way, I would like to thanks the sofa in our lab for accompanying me several nights in the lab.

I want to thank Professor Yu Hen Hu, Professor John A. Gubner, Professor Dieter Van Melkebeek, Professor Aditya Akella, Professor AnHai Doan for giving excellent classes, and take this opportunity to express my gratitude to all other the faculty and staff members in Electrical and Computer Engineering and Computer Sciences Department for their help and support.

Thank you to Yunting Tao, for all her love and support. Also, I wish to express my thanks to my friends at University of Wisconsin-Madison, Qiaoya Cui, Zuyu Zhang, Kaichen Zhao, Hanwen Chen, Luming Zhang, Xi Song, Gaoang Wang and so on. Bo Li at Washington University in St. Louis spent lots of his precious time during my Ph.D applications, and I want to thank him sincerely. I want to thank Karen Arneson, Linhui Yu, Rong Jiang, Huiyang Yu, Kun Gao, Xin Zhang and so on for their helps.

I would love to thank my dear parents Professor Yongde Wang and Yiqun Ha for their selfless and unconditional love. My father taught me to be persistent and encouraged me to pursue my dreams. My mother spent significant efforts to raise me alone, when I was a little boy, since my father was pursuing his Ph.D in another city. I wound also love to thank my grandparents, uncles, aunts, and cousins for their endless supports and encouragements. For this, I want to dedicate this thesis to them.

Contents

List of Figures

EXPLORING FULL-DUPLEX GAINS IN MULTI-CELL WIRELESS NETWORKS: A SPATIAL STOCHASTIC FRAMEWORK

Shu Wang

Under the supervision of Assistant Professor Xinyu Zhang
At the University of Wisconsin-Madison

Full-duplex radio technology is becoming mature and holds potential to boost the spectrum efficiency of a point-to-point wireless link. However, a fundamental understanding is still lacking, with respect to its advantage over half-duplex in multi-cell wireless networks with contending links. In this paper, we establish a spatial stochastic framework to analyze the mean network throughput gain from full-duplex, and pinpoint the key factors that determine the gain. Our framework extends classical stochastic geometry analysis with a new tool-set, which allows us to model a trade-off between the benefit from concurrent full-duplex transmissions and the loss of spatial reuse, particularly for CSMA-based transmitters with random backoff. The analysis derives closed-form expressions for the full-duplex gain as a function of link distance, interference range, network density, and carrier sensing schemes. It can be easily applied to guide the deployment choices during the early stage of network planning.

Xinyu Zhang

Abstract

Full-duplex radio technology is becoming mature and holds potential to boost the spectrum efficiency of a point-to-point wireless link. However, a fundamental understanding is still lacking, with respect to its advantage over half-duplex in multi-cell wireless networks with contending links. In this paper, we establish a spatial stochastic framework to analyze the mean network throughput gain from full-duplex, and pinpoint the key factors that determine the gain. Our framework extends classical stochastic geometry analysis with a new tool-set, which allows us to model a trade-off between the benefit from concurrent full-duplex transmissions and the loss of spatial reuse, particularly for CSMA-based transmitters with random backoff. The analysis derives closed-form expressions for the full-duplex gain as a function of link distance, interference range, network density, and carrier sensing schemes. It can be easily applied to guide the deployment choices during the early stage of network planning.

— 1 —

Introduction

1.1 Background

At early 1960s, Edward first proposed to apply stochastic geometry model to networks in his paper [1]. Since then, there is a significant amount of researches related to stochastic geometry for different wireless network technologies (*e.g. sensor networks*, *mobile ad hoc networks*, *cellular networks*). The corresponding models and analysis in these researches provide a better understanding of wireless network performance under different scenarios. For example, one can characterize random CSMA wireless networks [2] or non-slotted Aloha [3] wireless network. These works also help us to design current networks(*e.g.*, [4]), and even predict future networks.

The stochastic geometry in wireless networks can characterize the randomization of wireless network structure nature; the locations of the users in mobile or cellular networks, is quite random and is hard to predict. Therefore, such stochastic models are more flexible when dealing with the dynamic of wireless networks. Furthermore, these tools can provide closed-form or semi-closed-form expressions for different network matrix such as *signal-to-interference-plus-noise ratio*, *network throughput*.

Based on aforementioned merits, in this work, we first explore the

limitation of current stochastic geometry approaches. Then, we propose a new stochastic analysis framework for wireless network. Finally, we apply it to full-duplex wireless networks, which is a novel technique that allows wireless nodes to transmit and receive at the same time within single channel. Below we briefly describe the full-duplex background, and provide a primer on stochastic geometry.

1.1.1 Full Duplex Background

There is an increasing demand in on our limited wireless spectrum in recent years. By the year 2018, 61 % of all IP traffic will be Wi-Fi and mobile traffic, while wired traffic will only account for 39 % [5]. One the hand, the FCC recently released white space band as well as 60 Ghz band to relieve the spectrum crisis. One the other hand, researchers investigates different ways to improve current spectral efficiency. Among them, full-duplex networks gain a significant attention during these years.

This breakthrough technique defeats the long-held opinion among researchers that full-duplex wireless communication is infeasible. The main challenge of realizing full duplex is because of strong loopback self-interference between Tx chains and Rx chains. In general, this can be done by self-interference suppression, and people can achieve that through Digital cancellation, or Analog cancellation, or Antenna cancellation [6]. Recent advances in radio hardware and signal processing are pushing full-duplex wireless communications close to commercialization [7].

The full-duplex techniques will bring lot of benefits to future wireless network. Firstly, it greatly improved spectrum efficiency by factor of two theoretically, since it can transmit and receive simultaneously using the same channel. Secondly, it can use periodic feedback to inform the transmitter about the current channel state to perform the rate adaptation. Third, it can simplify communication initialization process, since RTS/CTS mechanism might not be necessary. Therefore, it can reduce the round trip

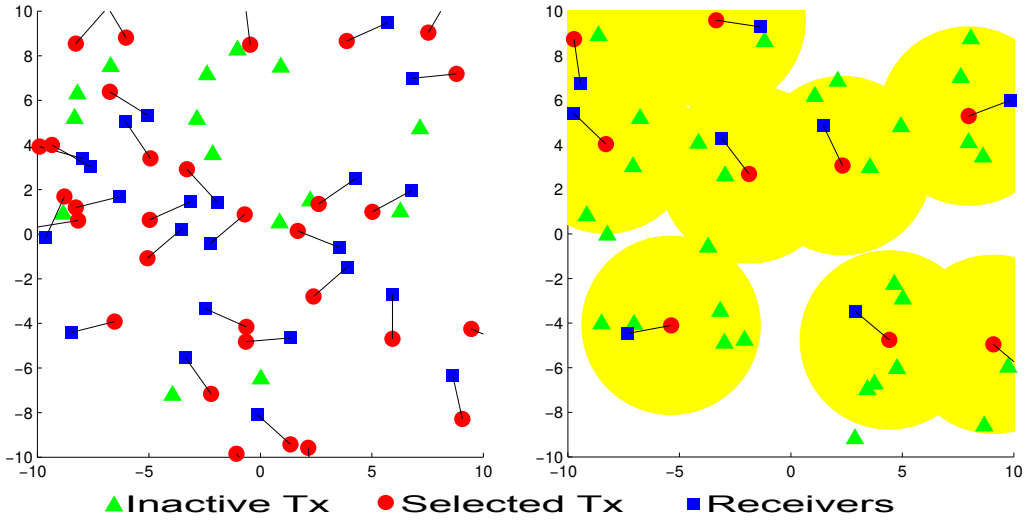

Figure 1.1: (L) ALOHA networks: TX initially distributed as a Poisson point process. (R) CSMA networks: Matèrn hard-core point process. The discs represent an exclusion zone around each transmitter because of carrier sensing process.

time and future reduce network congestion indirectly. Finally, it also bring some benefits to MAC layer design; there will be not hidden and exposed terminal problem since transmitter can continuous sense the channel.

1.1.2 Primer on Stochastic Geometry

Stochastic geometry provides average-case analysis of network, wherein the averages are made over a large number of nodes randomly located in the spatial domain. Most existing work focus on ALOHA networks and CSMA networks. The Fig. 1.1 shows a example of how to apply stochastic geometry to them.

Recent stochastic geometry models of 802.11 CSMA networks commonly apply a two-step approach [8]. *First*, nodes are assumed to be deployed following a Poisson Point Process (PPP). Then, the distribution of simultaneously active transmitters after CSMA contention is approx-

imated by a Matèrn hard core point process (HCPP). Simply put, the HCPP *thins* the parent PPP and models the winning nodes after random backoff. *Second*, the interference experienced by a typical winning node is approximated by the interference resulting from a PPP which has the same intensity as the HCPP. Such approximation has been shown to be fairly accurate, mainly because the exact locations of the active transmitters matter less than the number of other active transmitters (interferers) and their relative distances. Given the approximated HCPP, network performance metrics such as transmission success probability (under interference) and throughput can be easily derived. When applied to the ALOHA networks, stochastic geometry model has similar a two-step approach expect the CSMA contentions.

1.2 Motivations

Existing work mostly focused on full-duplex PHY-layer implementation [9, 10] or MAC protocols [11, 12] that extend 802.11 CSMA/CA. Unlike half-duplex wireless networks whose asymptotics have been investigated extensively [13], the fundamental network-capacity implications of full-duplex remain largely underexplored.

In distributed wireless networks, contending nodes' transmissions need to be separated in time, frequency, and/or space to avoid excessive interference. Whereas full-duplex allows a pair of nodes to co-locate their transmissions in the same time slot and frequency band, their spatial interference footprint is heavier than a half-duplex pair. An accurate characterization of this trade-off can lead to a fundamental understanding of the full-duplex network capacity and the achievable gain, thus guiding the practical protocol design and network deployment.

Furthermore, when applied to modeling the full-duplex gain, existing stochastic geometry models fall short of accuracy from three aspects.

(i) They mainly focus on potential transmitters through a homogeneous point process model. The spatial reuse between transmitters and receivers cannot be modeled but is the most critical factor that determines the full-duplex gain [14]. *(ii)* They assume a unit disk exclusive region around each transmitter, and omit the carrier sensing artifacts, such as exposed and hidden terminals, which again account for the discrepancies in theoretical and practical limit of both half-duplex and full-duplex networks. *(iii)* They commonly approximate the received signal-to-interference-plus-noise ratio (SINR) using the SINR at the transmitter side, yet whether a transmission succeeds depends SINR at the receiver side (or both sides for full-duplex).

We remedy the above limitations by marrying stochastic geometry with the two interference models proposed in Gupta and Kumar's seminal work on ad-hoc network capacity analysis [13].

1.3 Research Objectives and Contributions

The objective of this work is to provide an analytical framework allowing one to access the key properties of full-duplex wireless networks running carrier-sensing based random access protocols. The insights we seek to obtain include, *e.g.*, what is the network throughput (gain) when using full-duplex radios compared with half-duplex ones? What are the key factors that determine the gain and how to engineer such design knobs to maximize full-duplex's potential? With this framework, we also seek to derive general guidelines for deploying full-duplex multi-cell wireless LANs, *e.g.*, for an anticipated AP density, which type of radio is more cost-effective?

For such an analytical model, the main challenge lies in a need to take into account interference, random contention, and the resulting spatial reuse among contending links. Such factors, of course, are topology

dependent. One cannot traverse the enormous number of possible configurations, but must instead consider a statistical spatial model for the node locations, and extracts insights from there.

Following this principle, we assume certain statistical distribution of AP/client locations, and derive spatial averages of critical network quantities, *e.g.*, interference and spatial density of successful transmitters. Such a spatial averaging technique, widely referred to as *stochastic geometry* [15], has been used in a variety of wireless network examples, like ad-hoc networks, in order to perform average-case analysis of network throughput, by modeling the interference experienced by nodes under a random access MAC protocol.

It is, however, non-trivial to apply the classical stochastic geometry model to full-duplex networks, because of two new barriers. *First*, existing stochastic geometry analysis [8, 16] uses a hard-core point process (HCPP) to model the distribution of winning transmitters. The contention region of a point in HCPP is defined by a unit disc containing no other points. With full-duplex, the spatial footprint of two neighboring transmitters can become correlated, which can no longer be handled by conventional stochastic geometry models. *Second*, existing models only focus on winning transmitters after CSMA/CA contention, but ignore the receiver which itself has an exclusive region and is vulnerable to artifacts of carrier sensing such as hidden terminals. Such artifacts are critical to spatial reuse and to the real gain from full-duplex.

In light of the above challenges, we propose a new stochastic framework that can analyze the average spatial footprint of a *typical* full-duplex pair, as well as the spatial distribution of full-duplex pairs that win contention. Our approach leads to closed-form expressions for the average throughput of full-duplex networks with Poisson-bipolar distributed links. It also enables closed-form analysis of half-duplex throughput under carrier sensing artifacts, *e.g.*, hidden/exposed terminals. Consequently, we can

derive the full-duplex throughput gain under a variety of topological parameters and protocol imperfectness.

We find that the most critical factor that determines full-duplex gain is the mean link distance d relative to the carrier sensing range. A smaller d amplifies full-duplex gain since, intuitively, it reduces the interference footprint of a full-duplex link. For a fixed d, full-duplex gain tends to be larger in a very sparse deployment of APs, yet the gain saturates quickly as density increases. More interestingly, we found a major contributing factor to full-duplex gain lies in full-duplex nodes' capability to implicitly remove hidden/exposed terminals. Thus, the full-duplex gain tends to be amplified under imperfect carrier sensing. In addition, we show that our analytical framework can be applied to guide the choice between full-duplex or half-duplex technologies during deployment stage, given various objectives and constraints, *e.g.*, client/AP density and cost of half- and full-duplex radio.

1.4 Thesis Organization

The rest of this paper is structured as follows. We first present a background on our network models in Sec. 2. Then we analyze the full-duplex gain under two sets of interference models, in Sec. 3 and 4. In Sec. 5, we apply our models to full-duplex network planning. Sec. 6 discusses related work and finally, Sec. 7 concludes the thesis.

— 2 —

Overview of Network Model

2.1 Full-duplex Communication Model

A full-duplex node can simultaneously transmit and receive different packets. State-of-the-art full-duplex radio [10] can isolate the self-interference from transmitted signals to received ones, although perfect elimination is infeasible. Our analysis mainly focuses on the network-level impacts of full-duplex transmissions, assuming perfect full-duplex radio hardware.

When applied to multi-cell wireless LANs, full-duplex links can operate in two modes [9]. *Bidirectional transmission mode* (Fig. 2.1(a)) allows a pair of AP-client to transmit packets to each other simultaneously. *Cut-through transmission mode* (Fig. 2.1(b)) enables a full-duplex AP to simulta-

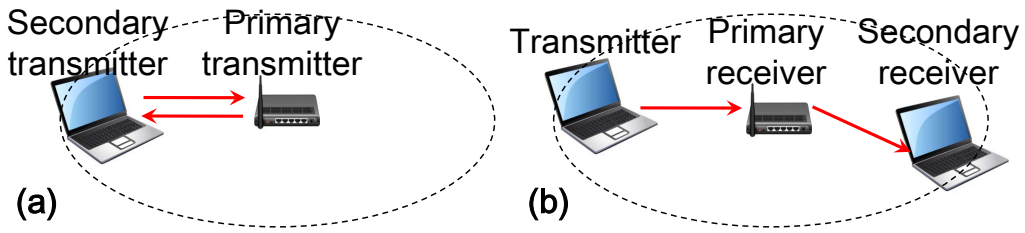

Figure 2.1: Full-duplex transmission modes in a wireless LAN: (a) bidirectional transmission and (b) cut-through transmission.

neously serve two clients, one for uplink and the other downlink. When applied to multi-hop networks, it is also referred to as wormhole relaying [14]. We first focus on the former mode, and then prove that the latter results in lower capacity (Sec. 3.4.2).

2.2 Network Topology Model

We model the locations of transmitters/receivers as some realizations of random point process. Unlike existing CSMA stochastic geometry analysis that commonly focus on Poisson-distributed transmitters (Fig. 2.2(a)), we model the transmitter *and* receiver locations using a *Poisson bipolar model* [17].

For a *half-duplex network*, transmitters are distributed following a PPP. Each transmitter T_X associates with a receiver R_X, located in a direction θ (Fig. 2.2(b)), random uniformly distributed in $[0, 2\pi)$. We first assume link distance is fixed to d, and then generalize our model to random link distance (Sec. 3.4). The links in a *full-duplex network* follow the same distribution, except that a receiver is a transmitter at the same time (assuming bi-directional transmission mode). We refer to the node that initialized the full-duplex transmission as *primary transmitter* T_1 and the other as *secondary transmitter* T_2.

Our model of a network with transmitter-receiver pairs can be considered as a snapshot of a multi-cell WLAN with multiple clients per cell, wherein every AP is communicating with one associated client at any one time instant. Over time, the network can be considered as realization of multiple snapshots, and its performance mainly depends on the mean spatial throughput (density of successful transmissions) in each snapshot.

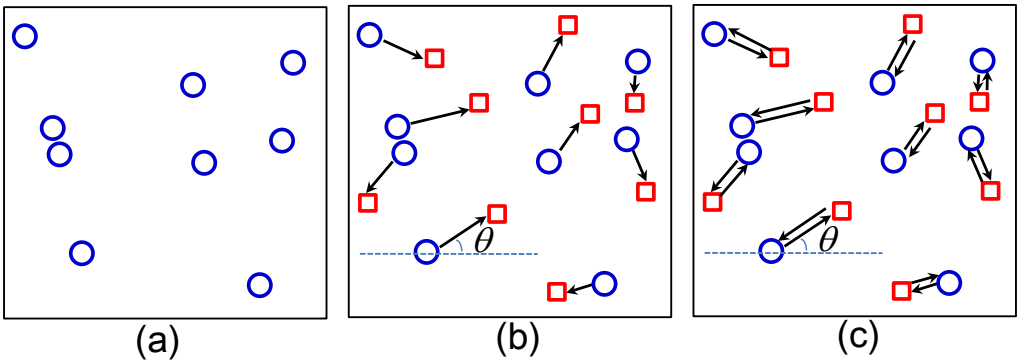

Figure 2.2: (a) Existing stochastic model widely assumes Poisson distributed potential transmitter *nodes*. (b) Our half-duplex model focuses on *links* with Poisson bipolar model with mean link distance d. (c) Our full-duplex model focuses on bi-directional transmission *links*.

2.3 Contention Models

MAC protocols(e.g. ALOHA, CSMA) provide medium access control mechanism so that multiple network nodes can access the shared channel simultaneously. In other worlds, the network nodes need to content with each other to obtain the privilege to access medium. To characterize different MAC protocol, we consider two typical contention models in our analysis, unslotted ALOHA and CSMA-based network.

2.3.1 ALOHA Networks

In an ALOHA network, every node can access the channel independently with a certain probability p_m without checking current channel state. Because of this random approach, the maximum throughput is 18.4% for unslotted ALOHA, and 37% for slotted ALOHA comparing with the optimal one. The fundamental reason for the low throughput is excessive collisions due to the random access. The simplicity of this mechanism makes it easy to be analyzed, and ALOHA plays an important and fundamental role for other MAC protocol analysis.

2.3.2 CSMA-based Networks

In CSMA-based network, this problem is partially solved by a simple idea: listening the channel before transmitting;if the channel is busy, then the transmission will be deferred, and a collision will be avoided. This mechanism greatly improve the wireless network performance,and one modification version called CSMA with collision avoidance is a part of current IEEE 802.11 wireless MAC standard. In our model, we consider different sensing models separately in Sec. 3, and analyze how it affect network throughput.

2.4 Interference Models

Our analytical framework inherits the simplicity of the interference models from Gupta and Kumar [13], but enhances them with a stochastic geometry model of random CSMA contention.

2.4.1 Protocol Model

In the protocol model, each transmitter has a fixed transmission range, interference range, and carrier sensing range. For simplicity, the interference and carrier sensing range are assumed to be the same value R_I, whereas the transmission range R_S can be smaller. A successful transmission depends on two conditions: *First*, the transmitter can be activated after carrier sensing and contention(discussed in 2.3), *i.e.*, the transmitter has the lowest backoff counter among all candidates it can sense. Effectiveness of the carrier sensing depends on the sensing models, and will be treated case-by-case in Sec. 3. *Second*, no other concurrent transmitters are activated within the corresponding receiver's interference range.

2.4.2 Physical Model

The physical model differs in the second condition. Instead of a fixed interference range, the transmission succeeds only if the link SINR exceeds a threshold β. The interference power is the cumulative interference from all concurrent transmitters, which still exist outside the transmitter's carrier sensing range after CSMA contention. We defer the formal mathematical definition to Sec. 4.

— 3 —

Full-duplex Gain Under the Protocol Model

In this section, we describe our stochastic geometry framework that establishes a closed-form analysis of full-duplex gain under the protocol interference model. The analysis derives the spatial throughput of two different network models: ALOHA networks and CSMA-Like networks. In ALOHA network, because there is no carrier sensing process, we only need to consider full-duplex and halp-duplex networks. However, in CSMA-Like networks, the wireless networks are also depended on contention models. Therefore, we need will consider four different network models: : full-duplex; half-duplex with perfect carrier sensing, imperfect carrier sensing, and RTS/CTS. In each case, the analysis follows two major steps: *(i)* analyze the *mean contention region* around a *typical* pair of nodes. *(ii)* derive the probability of successful transmission for the typical pair that runs the CSMA random backoff, given the Poisson bipolar distributed contending links within its mean contention region. Then we compute and compare the full-duplex spatial throughput with all the half-duplex models to obtain the full-duplex gain in each case.

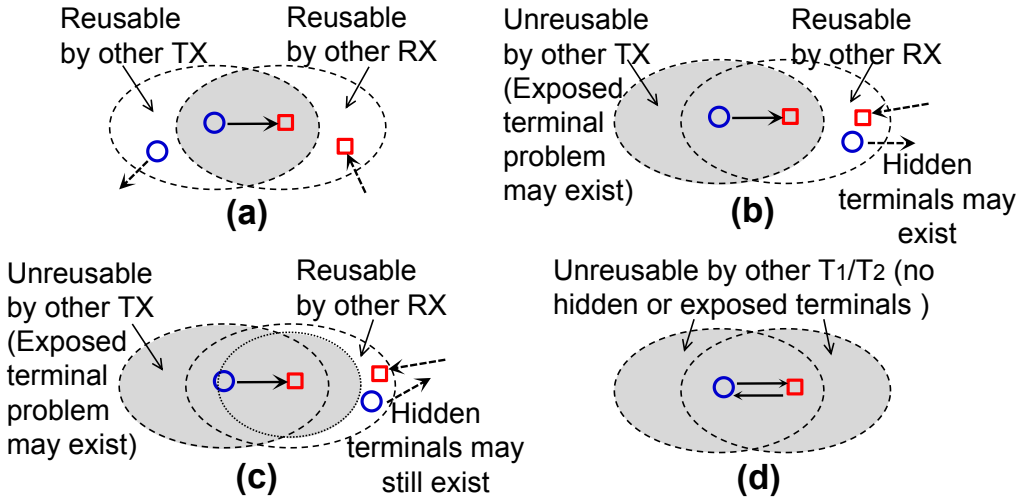

Figure 3.1: Spatial reuse effects due to carrier sensing: (a) half-duplex networks with perfect carrier sensing; (b) half-duplex networks with imperfect carrier sensing; (c) RTS/CTS reduces hidden terminals but does not completely remove them; (d) full-duplex results in perfect carrier sensing. To simplify the illustration, we assume interference range and carrier sensing range overlap.

3.1 Mean Contention Region (MCR)

We first introduce a novel analytical technique called mean contention region (MCR) that overcomes the aforementioned limitations of classical stochastic geometry models.

Definition: Given a typical link $\mathcal{L}_o$ and a bounded region $\Omega \in \mathbb{R}^2$ around $\mathcal{L}_o$. We arbitrarily partition Ω into n small regions represented by their areas: $\Delta\Omega_1, \Delta\Omega_2, \cdots, \Delta\Omega_n$. Let $\sigma = \max_{1 \leqslant j \leqslant n} \Delta\Omega_j$. We randomly select a point X_i from region $\Delta\Omega_i$, and define the *Mean Contention Region* as,

$$\lim_{\sigma \to 0} \sum_{i=1}^{n} p(X_i)\Delta\Omega_i, \tag{3.1}$$

where $p(X_i)$ is the probability that a transmitter of another link $\mathcal{L}_i$ located

at X_i contends with typical link $\mathcal{L}_o$. If the limit exits and is unique, then we can cast it as: $\int_\Omega p(X)d\Omega$. Since $p(X)$ is a continuous function on a bounded region, the integral exists and is finite. □

Intuitively, MCR represents a spatial average of the area within which contenders/interferers may be located. Since the link locations follow a stationary distribution, it suffices to analyze the MCR of a *typical* link $\mathcal{L}_o$, comprised of a transmitter and a receiver (or two full-duplex bi-directional transmitters).

3.1.1 ALOHA Networks

In ALOHA networks, we only need to consider half-duplex and full-duplex network separately. For half-duplex networks, at any time, the successful transmission only happens when *there is not other receiver within transmitter's interference range, and no other transmitter within receiver's interference range*. Essentially, this condition is the same as that in half-duplex with perfect carrier sensing in CSMA networks. Therefore, in such two scenarios, they share the same spatial reuse region, and thus the same MCR. Similarly, full-duplex ALOHA and CSMA networks have the same MCR as well. We defer the related MCR calculation in Sec. 3.1.2.1 and Sec. 3.1.2.4.

3.1.2 CSMA-based Networks

For CSMA networks, the definition of contenders/interferers, and the corresponding $p(X)$, depend on not only the duplex mode, but also the carrier sensing. Hence the MCR needs to be analyzed separately, for the 4 categories below.

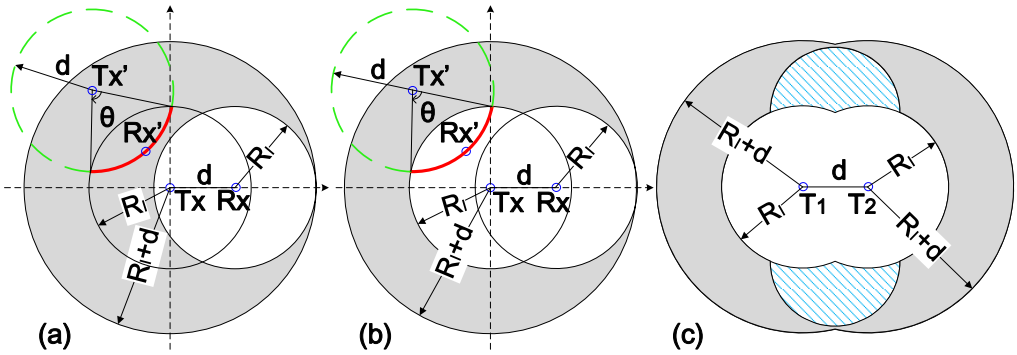

Figure 3.2: Analyzing mean contention region of : (a) half duplex network with perfect carrier sensing, (b) half duplex network with imperfect carrier sensing and (c) full duplex network.

3.1.2.1 Half-duplex with Perfect Carrier Sensing

Perfect carrier sensing assumes perfect knowledge of contenders: each transmitter is well aware of which receivers it interferes with and which transmitters interfere with its receiver. Therefore, there exist no hidden/-exposed terminals and spatial reuse is perfect (Fig.3.1(a)). This model is especially useful considering the recent advances in cross-layer implementation that minimizes the impact of hidden [18] and exposed terminals [19]. It is also the basic assumption behind Gupta and Kumar's protocol model for CSMA networks [13]. The following theorem offers a closed-form characterization of the corresponding MCR. For simplicity of exposition, we only provide the essential steps behind our analysis.

Theorem 3.1. *The mean contention region for half-duplex CSMA networks with perfect carrier sensing is given by*

$$V_{HP} = \pi R_I^2 + \frac{2}{\pi}\int_{R_I-d}^{R_I+d} (\pi - \theta)\theta r dr \tag{3.2}$$

$$\theta = \arccos\left(\frac{d^2 + r^2 - R_I^2}{2dr}\right).$$

Proof sketch: Consider a typical link $\mathcal{L}_o$ whose transmitter T_X is located at the origin and its receiver at distance d along the x-axis (Fig. 3.2(a)).

First, the receiver's interference range (white area in Fig. 3.2(a)) should be counted deterministically within MCR (first term on the RHS of Eq. (3.2)), because any transmitter from other contenting link $\mathcal{L}'$ therein will contend with the typical link $\mathcal{L}_o$.

Second, consider a contending link $\mathcal{L}'$ whose transmitter $T_{X'}$ is within the shaded area in Fig. 3.2(a). If its receiver $R_{X'}$ is located within the interference range of T_X (red solid arc), then $R_{X'}$ will be interfered. Otherwise (green dashed arc), it needs not contend with the typical link and can transmit concurrently under perfect carrier sensing. Under Poisson bipolar model, the orientation of a receiver *w.r.t.* its transmitter is uniformly distributed in $[0, 2\pi)$. Thus, we can obtain the probability of $R_{X'}$ located in T_X's interference range by calculating the ratio of θ to 2π. Since this probability $p(X)$ depends on the transmitter's location, we can integrate the probability throughout the shaded area to obtain the spatial average (second term on the RHS of Eq. (3.2)).

For any other transmitter outside the above two regions, its receiver $R_{X'}$ can never fall within T_X's interference range, and thus it should not be counted into the MCR. □

3.1.2.2 Half-duplex with Imperfect Carrier Sensing

In the basic 802.11 protocol (Fig. 3.1(b)), a node defers its transmission whenever it senses a busy channel. This mechanism reduces the risk of collision but often leads to the *exposed terminal* problem, *i.e.*, some nodes may not interfere a receiver, but are unnecessarily suppressed by the corresponding transmitter. In addition, it suffers from the *hidden terminal* problem, *i.e.*, other nodes outside the ongoing transmitter's carrier sensing range but inside the ongoing receiver's interference range can still cause collisions. We refer to this category of protocol as *imperfect carrier sensing*,

and analyze the MCR as follows.

Theorem 3.2. *Under imperfect carrier sensing, the mean contention region for CSMA networks is given by*

$$V_{HI} = V_u + \frac{2}{\pi}\int_{R_I}^{R_I+d} (\pi - \theta)\theta r dr \tag{3.3}$$
$$V_u = 2\pi R_I^2 - 2R_I^2 \arccos(\frac{d}{2R_I}) + d\sqrt{R_I^2 - \frac{d^2}{4}}$$
$$\theta = \arccos\left(\frac{d^2 + r^2 - R_I^2}{2dr}\right)$$

Proof sketch: The transmitter T_X suppresses all other transmitters within its interference range which, together with the receiver's interference range, become a deterministic contention region (the V_u term above, corresponding to the white region in Fig. 3.2(b)). Spatial average of contention region for the shaded area can be derived in a similar way to Theorem 3.1. □

3.1.2.3 Half-duplex with RTS/CTS Signaling

An enhanced version of 802.11 uses RTS/CTS to alleviate hidden terminals (Fig. 3.1(c)). Yet it still bears the exposed terminal problem. Moreover, there may still be hidden terminals outside the CTS transmission range but within the receiver's interference range. Denote the transmission range as R_S, then we can derive the MCR under RTS/CTS signaling as follows.

Theorem 3.3. *The mean contention region for half duplex network using RTS/CTS is given by*

$$V_{HRC} = \begin{cases} V_1 + V_2 + V_3 + 2(V_4 - V_5) & d > R_I - R_S \\ V_{HI} & d \leqslant R_I - R_S \end{cases} \tag{3.4}$$
$$V_1 = 2\pi R_I^2 - 2R_I^2 \arccos(\frac{d}{2R_I}) + d\sqrt{R_I^2 - \frac{d^2}{4}}$$
$$V_2 = \frac{2}{\pi}\int_{R_I}^{R_I+d} (\pi - \gamma_1 - \theta_2)\theta_1 r dr$$

$$V_3 = \frac{2}{\pi}\int_{R_I}^{R_S+d} (\pi - \gamma_2 - \theta_3)\theta_4 r dr$$
$$V_4 = \frac{1}{2\pi}\int_0^d \int_{\theta_5-\gamma_2}^{\pi-\theta_6+\gamma_1} (\varphi_1 + \varphi_2 + \varphi_3) r dr d\theta$$
$$V_5 = \frac{1}{2\pi}\int_{R_S}^{R_I} \int_{\pi-\theta_1}^{\pi-\gamma_2-\theta_3} (\varphi_4 + \varphi_5 + \theta_4) r dr d\theta$$

The γ_1, γ_2, θ_1 to θ_5 and φ_1 to φ_5 are intermediate parameters. Detailed expressions are put in Appendix A.1 for simplicity of exposition.

The proof follows similar steps as the full-duplex case below, and is thus omitted to avoid redundancy.

3.1.2.4 Full-duplex

For full-duplex links, we assume a carrier sensing model similar to the FuMAC in [20]. A bi-directional full-duplex transmission can start only if both the primary and secondary transmitter sense an idle channel. Such synchronous full-duplex scheme has proven to have superior performance than one that mixes half-duplex with full-duplex transmissions [20]. In addition, *(i)* it eliminates hidden terminals because every receiver is a transmitter at the same time that uses its transmission as a busy-tone to protect itself from interferers. *(ii)* exposed terminals no longer exists, because no transmitter can coexist with other transmitter (and simultaneously a receiver) within the carrier sensing range anyway (Fig. 3.1(d)).

In other words, *full-duplex carrier sensing implicitly removes the hidden/-exposed terminals*. Our later analysis will show that this is where the main benefit of full-duplex comes from. Under this protocol, the MCR can be characterized as follows.

Theorem 3.4. *The mean contention region for a typical full-duplex link is given by*

$$V_F = V_1 + 2V_2 + 2V_3 \tag{3.5}$$

$$V_1 = 2\pi R_I^2 - 2R_I^2 \arccos(\frac{d}{2R_I}) + d\sqrt{R_I^2 - \frac{d^2}{4}}$$
$$V_2 = \frac{2}{\pi}\int_{R_I}^{R_I+d} (\pi - \theta_2 - \theta_3)\theta_1 r dr$$
$$V_3 = \int_0^d \int_{\frac{2\theta_4 + \theta_5 - \pi}{2}}^{\frac{3\pi - 2\theta_4 - \theta_5}{2}} (\frac{\varphi_1 + \varphi_2 + \varphi_3}{2\pi}) r dr d\theta$$

where θ_1 *to* θ_5, φ_1 *to* φ_3, *and* δ_1 *to* δ_2 *are intermediate parameters whose detailed expressions are available in Appendix A.2.*

Proof sketch: We consider three regions shown as different patterns in Fig. 3.2(c). The white region is a deterministic contention region, whereas other two contribute to the MCR probabilistically, and can be analyzed using a similar procedure as in Theorem 3.1. The detailed proof is put in Appendix A.2. □

3.2 Spatial Density of Successful Transmissions

We now derive the mean transmission density, *i.e.*, average number of successful transmissions per unit area, after the typical pair of nodes *contend* with peers in the MCR.

For the ALOHA networks (Sec. 2.3.1), it can be modeled as a Matèrn Type I process [17] that *thins* the original PPP distributed based on medium access probability p_m. The *Palm retaining probability* that a point x of the process is retained after Matèrn Type I thinning and independent medium access is given by $e^{-\mu p_m V}$, where μ is the density of original PPP.

The CSMA contention (Sec. 2.3.2) can be modeled as a Matèrn Type II process ([21]) that *thins* the original PPP distributed contenders within the MCR. Given a stationary independently marked PPP of intensity μ, the *Palm retaining probability* that a point x of the process having mark t is

retained after Matèrn Type II thinning is given by $e^{-\mu t V}$, where V is the contention area [22].

We adapt this result to our analysis and obtain the density of successful transmissions in the aforementioned 6 cases for both ALOHA networks and CSMA-based networks. Unlike existing work for ALOHA networks widely consider interference around transmitter side, our work is more close to the reality in the sense that we focus on receiver side. Besides, their work widely uses a deterministic unit disk to model V, whereas our MCR model enables a spatial average analysis of the contention region that can model all 4 cases for CSMA-base networks. In the following section, we will first discuss spatial density of ALOHA networks and CSMA-based networks.

3.2.1 ALOHA Networks

3.2.1.1 Half-duplex Model

We assume λ_p be the original deployment density of all potential transmitter, and each transmitter independently decide to access the medium with probability p_m. Therefore, all the active transmitters is still a PPP with density $p_m\lambda_p$. Therefore, the probability of the typical successful half-duplex pair is given by:

$$\lambda_{HA} = \exp(-p_m\lambda_p V_{HP}) \tag{3.6}$$

3.2.1.2 Full-duplex Model

In the full-duplex model, we assume the primary and secondary transmitters access the medium at the same, which can be realized using handshake protocols like [20]. Similarly, the probability of the typical successful full-duplex pair is given by:

$$\lambda_{FA} = \exp(-p_m \lambda_p V_F) \tag{3.7}$$

3.2.2 CSMA-based Networks

3.2.2.1 Half-duplex Models

Let λ_p be the original deployment density of all potential transmitters. For the perfect carrier sensing case, the probability of the typical pair winning contention is $\exp(-\lambda_p t V_{HP})$, where V_{HP} follows Theorem 3.1. The mean successful density after contention can be obtain by averaging over all possible backoff counter t as:

$$\lambda_{HP} = \lambda_p \int_0^1 e^{-\lambda_p V_{HP} t} dt = \frac{1}{V_{HP}} \left(1 - e^{-\lambda_p V_{HP}}\right) \tag{3.8}$$

Similarly, we can derive the successful transmission density for the imperfect carrier sensing case and RTS/CTS case as:

$$\lambda_{HI} = \frac{1}{V_{HI}} \left(1 - e^{-\lambda_p V_{HI}}\right), \text{and } \lambda_{HRC} = \frac{1}{V_{HRC}} \left(1 - e^{-\lambda_p V_{HRC}}\right)$$

3.2.2.2 Full Duplex Model

For a full-duplex bi-directional link, we assume the primary and secondary transmitters hold the same backoff counter t, which can be realized using handshake protocols like [20]. Suppose t follows the same uniform distribution as in the half-duplex case, then the mean successful density of full-duplex transmissions is:

$$\lambda_F = V_F^{-1} (1 - e^{-\lambda_p V_F}). \tag{3.9}$$

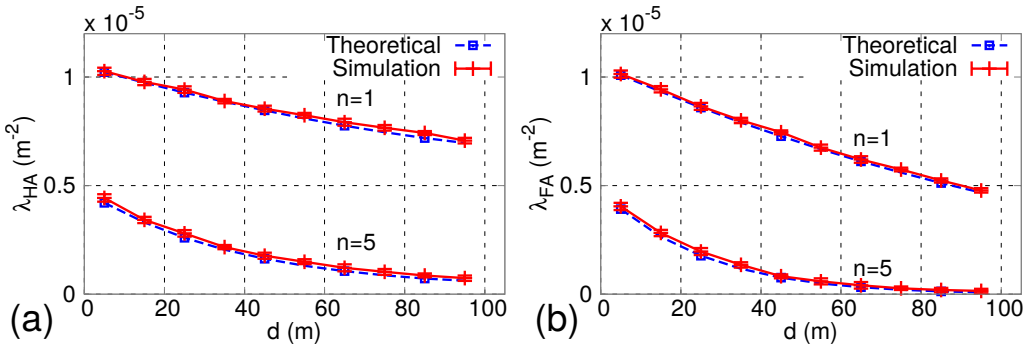

Figure 3.3: Successful transmission density vs. link distance for (a). half-duplex and (b). full-duplex in ALOHA networks $R_I = R_C = 100, p_m = 0.6$.

3.2.3 Simulation Verification

To verify the accuracy of the above closed-form models, we implement a simulator that simulates the carrier sensing, contention, and collision (due to hidden terminals) behaviors of each of the four network scenarios. The simulator runs in a round-based manner, and outputs the links that successfully transmit in each round. We run 20 randomly generated topologies with Poisson bipolar link distribution within a 100 km^2 region. Interference range $R_I = 100$m (equals carrier sensing range R_C) and link distance d ranges from 0 to R_I. We assume p_m is 0.6 for ALOHA networks. We simulate a sparse network with per-node *neighbor density* of $n = 1$ and dense network with $n = 20$. The corresponding deployment density is $\lambda_p = n/(\pi R_I^2)$.

Fig. 3.4 and Fig. 3.3 compare the simulation results with the closed-form model. We see that our analytical results match closely with the simulated average across all the cases. In general, the successful transmission density decreases as d approaches R_I, because a longer link-distance is more vulnerable to interference and contention. This is true for both ALOHA and CSMA-based networks.

The successful transmission density of the ALOHA networks drops

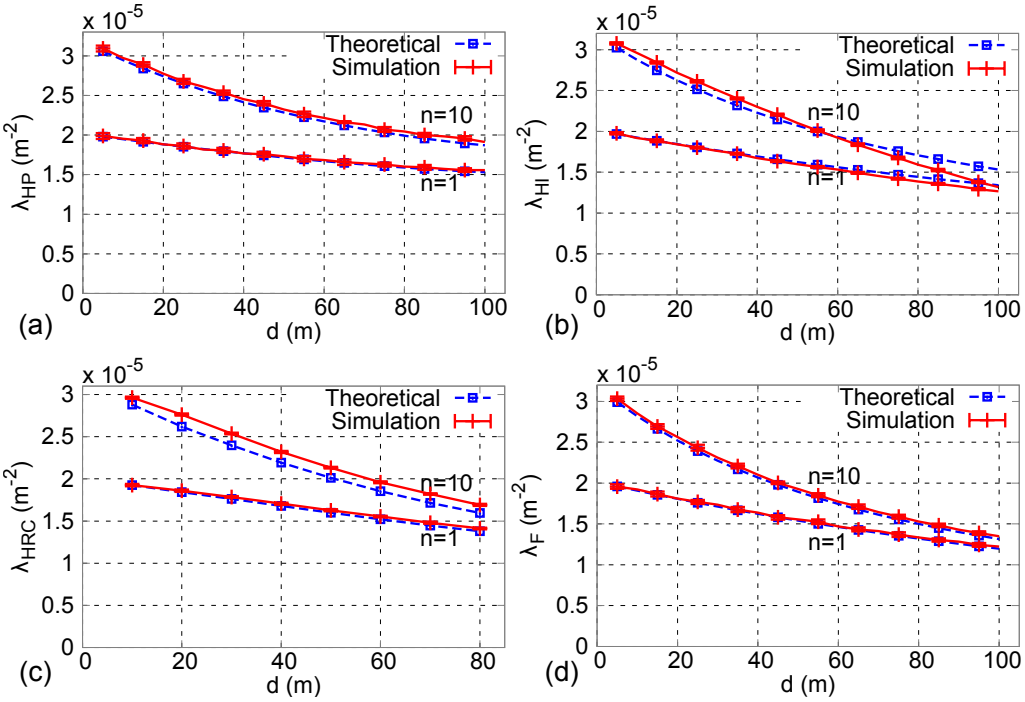

Figure 3.4: Successful transmission density vs. link distance for half-duplex CSMA networks with: (a) perfect carrier sensing; (b) imperfect carrier sensing; (c) RTS/CTS; and (d) Full-duplex CSMA networks. $R_I = R_C = 100, R_S = 80$.

much than that of CSMA-based networks when d increases. The ALOHA networks is much more vulnerable than CSMA-based network, since there is not any mechanism to protect the transmission. For half-duplex in CSMA-based networks, perfect carrier sensing results in higher density than the other two cases. RTS/CTS alleviates hidden-terminals, but the protection sacrifices spatial reuse, and results in similar density as the imperfect carrier sensing. Although the density of full-duplex pairs is similar to that of half-duplex when d is small, it decreases faster, implying that it is more vulnerable to loss of spatial reuse as d increases.

We proceed to analyze the impacts of the successful transmission density on full-duplex gain.

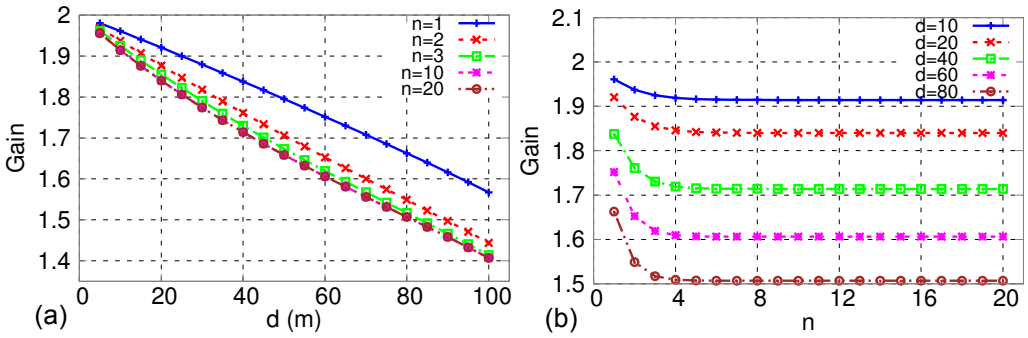

Figure 3.5: Full-duplex gain over half-duplex network with perfect carrier sensing.

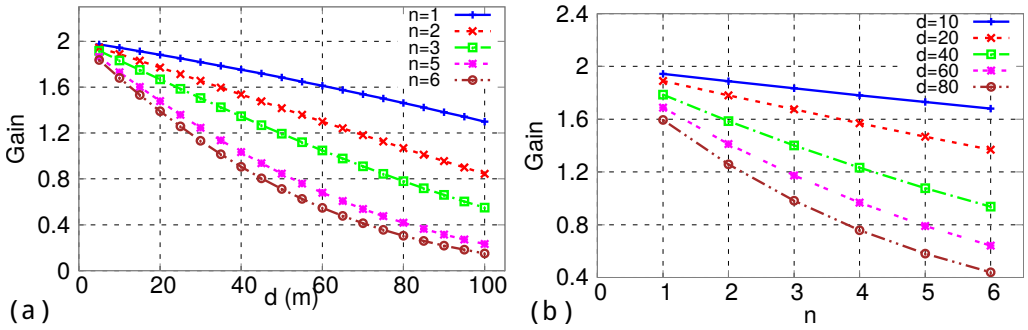

Figure 3.6: (a) Gain of full-duplex over half-duplex ALOHA networks vs. link distance (d) for several n, where $n/\pi R_I^2 = \lambda_p$ (b) Gain of full-duplex over half-duplex ALOHA networks vs. n for several values of link distance d

3.3 Throughput and Full-duplex Gain

The mean density of successful transmissions can be regarded as spatial-average of the network throughput, which also equals its time-average across stationary topology realizations (Sec. 2.2). Therefore, we can derive the full-duplex throughput gain over half-duplex perfect carrier sensing as: $G_{HP} = 2\lambda_F/\lambda_{HP}$, where a multiplier factor 2 is needed since each full-duplex pair supports double link transmission. The gain over other half-duplex cases in CSMA-based networks and ALOHA follows the same derivation.

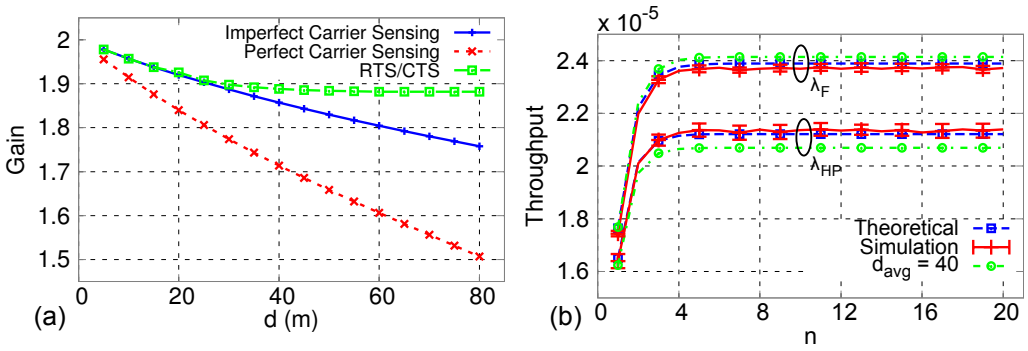

Figure 3.7: (a). Gain under different carrier sensing schemes of half duplex network (b).Density of Successful Transmissions under $d \sim unif[0, 80]$ for Half-duplex networks with perfect carrier sensing and Full-duplex CSMA networks.

In Fig. 3.6, we show the full-duplex gain in ALOHA networks under the same simulation settings. It is clear that when link distance d increases to R_I, the gain drops quickly towards 0. The fundamental reason behind this is the full-duplex networks are much more vulnerable than half-duplex networks, since both primary and secondary transmitters might suffer from interference. This becomes more significant when either link distance b or density n increases.

From this analytical insights, we can conclude that *under the protocol interference model and ALOHA, the full-duplex gain is between 0% to 200%, and full-duplex networks are much more vulnerable than half-duplex networks.*

We plot the analytical full-duplex gain for all cases in Fig. 3.7, using similar parameters as above (Note that $R_I = R_C = 100$m). A common observation is that the gain may be close to 2 when d is near 0, but decreases as d approaches R_I. The reason behind is the same as the decreasing transmission density as discussed above. Fig. 3.5 also shows that the deployment density λ_p has minor impact under perfect carrier sensing: for a given d, the gain quickly saturates as λ_p increases. We found the imperfect sensing and RTS/CTS cases show similar behavior.

Among all cases (Fig. 3.7(a)), the gain drops fastest in the perfect carrier

sensing case. The underlying reason can be understood from Fig. 3.1(a). For a half-duplex network with perfect carrier sensing, as d approaches R_I, a larger fraction of space can be reused by neighboring links, which diminishes the full-duplex's advantage in concurrent transmissions. The trend is consistent with the protocol model in [14]. On the other hand, the imperfect carrier sensing and RTS/CTS cannot fully take advantage of the spatial reuse, thus amplifying the full-duplex gain at larger d. We found that for the largest d ($d = R_I$) in the former two cases, the full-duplex gain is 1.4 and 1.71, and for the largest d ($d = R_S$) in the RTS/CTS case it is 1.88.

From the above analytical insights, we can conclude that *under the protocol interference model and CSMA contention model, the full-duplex gain is between 140% to 200%, and it largely comes from full-duplex's capability to overcome the imperfect carrier sensing in half-duplex.*

3.4 Discussion

3.4.1 Beyond Fixed Link Distance

All the analysis above has assumed the same fixed distance d for all links. We now show that the spatial average throughput is the same as that under a random uniformly distributed link distance with mean d.

Denote the link distance of the typical link as r_1 and a contending link as r_2. Unlike the previous MCR analysis, we should calculate the MCR *conditioned on* r_1 and r_2. Denote the corresponding MCR as $V(r_1, r_2)$. Suppose link distance is uniformly distributed from $[0, R_S]$, where R_S is the transmission range, we can obtain the density of successful transmission by averaging over all possible r_1 and r_2 as,

$$\frac{1}{R_S^2}\int_0^{R_S}\int_0^{R_S}\frac{1-e^{-\lambda_p V(r_1,r_2)}}{V(r_1,r_2)}dr_1 dr_2 \tag{3.10}$$

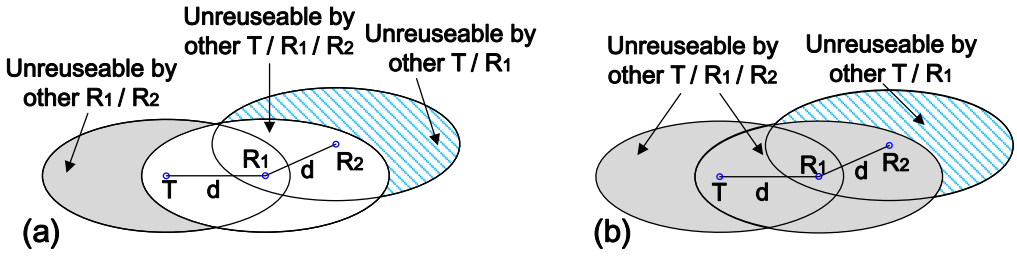

Figure 3.8: Cut-through transmission with (a) Perfect carrier sensing (b) Imperfect carrier sensing.

This applies to both the full-duplex and half-duplex cases. To verify the approach, we compare the resulting transmission density with simulation, following similar setup as in the fixed-d case (Sec. 3.2.3). The results in Fig. 3.7(b) show that the simulation results are in close agreement with Eq. (3.10). We only show perfect carrier sensing for half-duplex, without loss of generality. Given R_S =80m, and hence mean link distance 40m, we also compare the result from our previous fixed distance model for $d = 40$ with that of the uniformly distributed case in Fig. 3.7(b) and we can see that the results match closely.

3.4.2 Full-duplex Cut-Through Transmission Mode

Using some elements of the foregoing analysis, and by extending the Poisson Bipolar model, we now prove that the cut-through transmission is always inferior to the bi-directional transmission mode. Denote the transmitter T, primary receiver R_1 and secondary receiver R_2 (Fig. 2.1) using their locations X_i, Y_i and Z_i, respectively. We assume the X_i follows a PPP; Y_i is at distance d with a random orientation θ_i uniformly distributed in $[0, 2\pi)$. γ_i denotes the orientation of the secondary receiver *w.r.t.* the primary receiver. Since we need to ensure that Z_i is not interfered by X_i, the range of link distance d should be $[\frac{R_I}{2}, R_I]$ and the range of γ_i should be $[\theta - \arccos(\frac{R_I^2}{2d^2} - 1), \theta + \arccos(\frac{R_I^2}{2d^2} - 1)]$ in which it is uniformly distributed.

Similar to the bi-directional full-duplex model we assume X_i and Y_i have the same back-off counter, which are uniformly distributed in $[0, 1)$. With this model setup, we can prove that:

Proposition 1. *The network throughput under bi-directional transmission mode is no smaller than that of cut-through transmission mode with either perfect/imperfect carrier sensing.*

Proof sketch: Based on Fig. 3.8 we elucidate the spatial occupation of cut-through transmission. Observing both the transmitter and secondary receiver operate in half-duplex, we prove that adding both of their MCR to the primary receiver's MCR will exceed MCR of a bi-directional transmission pair, with either perfect or imperfect carrier sensing. So the network throughput is lower or equal. We put a detailed proof in Appendix A.3. □

— 4 —

Full-duplex Gain under the Physical Model

In this section, we first obtain a lower bound on the successful transmission probability of a half-duplex link under the physical model, which is shown to be tight through simulation. We only focus on the imperfect carrier sensing (basic 802.11) case. Extension to other half-duplex cases is trivial and omitted. Then, we derive an approximation of the full-duplex links' successful transmission probability, and subsequently obtain the full-duplex network throughput gain. Our analysis is built on the *Campbell's* theorem [23], *second-order product density* of a stationary point process and *Jensen's* inequality.

4.1 Modeling Transmission Success for Half-duplex

Usually, the nearby interference is much higher than the noise power [15]. Therefore, for a typical link, the successful transmission probability equals the probability that its signal-to-interference ratio (SIR) exceeds a threshold β, conditioned on this link wins the CSMA contention.

4.1.1 Modeling Contention and SIR

We leverage the Matèrn Type II point process [24] to model the winning transmitters in half-duplex CSMA contention. A transmitter of the original deployed PPP $\tilde{\Phi}_o$ is chosen for the Matèrn process if it has the least backoff counter among all other points that lie in its carrier sensing range R_C. Denote Φ_m^H as the thinned point process after all winning transmitters are chosen, then its intensity is [25]:

$$\lambda_m^h = \frac{1 - e^{-\lambda_p \pi R_C^2}}{\pi R_C^2} \tag{4.1}$$

where λ_p is the intensity of $\tilde{\Phi}_o$, *i.e.*, the deployment density.

For a winning transmitter X_i, the receiver Y_i can successfully decode its packets only if its SIR satisfies:

$$SIR_{Y_i} := \frac{P h_{X_i Y_i} d^{-\alpha}}{\sum_{X_j \in \Phi_m^H, j \neq i} P h_{X_j Y_i} \|X_j - Y_i\|^{-\alpha}} > \beta \tag{4.2}$$

where P represents the transmission power and h_{XY} represents the channel fading coefficient from a transmitter X to a receiver Y. We assume the *Rayleigh* fading model, in which the $\{h_{XY}\}$ are a set of *i.i.d.* exponentially distributed random variables with mean $\mathbb{E}(h_{XY}) = 1$. The *path loss* from a node x to a node y is given by $\|x - y\|^{-\alpha}$, where $\|x - y\|$ is the *Euclidean* distance between the nodes and α is the path loss exponent.

4.1.2 Successful Transmission Probability

We again consider a *typical* transmitter $X_o \in \Phi_m^H$, located at the origin *o*, and receiver Y_o at a distance d with orientation ϕ uniformly distributed in $[0, 2\pi)$. Then we calculate the probability in Eq. (4.2) under the *Reduced Palm distribution* $\mathbb{P}^{!o}_{\Phi_m^H}$ of Φ_m^H. $\mathbb{P}^{!o}_{\Phi_m^H}(SIR_{Y_o} > \beta)$ denotes the probability that

the SIR at receiver is greater than β given that $X_o \in \Phi_m^H$, but not counting X_o's transmission as interference. With this setup, we can have:

Theorem 4.1. *Under the physical model, the successful transmission probability for a typical Poisson bipolar distributed half-duplex link can be bounded as:*

$$\mathbb{P}^{!o}_{\Phi_m^H}(SIR_{Y_o} > \beta) > \frac{1}{2\pi}\int_0^{2\pi} exp\left\{-\frac{\lambda_p^2}{\lambda_m^h}\int_0^{\infty}\int_0^{2\pi} k(r,\theta)\Delta(r,\theta,\phi)rdrd\theta\right\}d\phi.$$

where $k(r,\theta)$ *denotes the probability that two transmitters of* $\tilde{\Phi}_o$ *separated by a distance* r *and having a phase angle difference* θ *are retained in* Φ_m^H *and is given in [25].* $V(r)$ *is the union of areas covered by the carrier sensing ranges of the two transmitters separated by a distance* r *and is given by*

$V(r) = 2\pi {R_C}^2 - 2{R_C}^2 \arccos(\frac{r}{2R_C}) + r\sqrt{{R_C}^2 - \frac{r^2}{4}}, 0 \leqslant r \leqslant 2R_C$

and, $\Delta(r,\theta,\phi) = \ln\left(1 + \beta\left(\frac{d^2}{r^2+d^2-2dv\cos(\theta-\phi)}\right)^{\frac{\alpha}{2}}\right)$.

Proof: Available in the Appendix A.4. □

Fig. 4.1(a) compares the lower-bound with our simulation results across 20 topologies. We observe that the bound matches tightly with the simulated mean successful transmission density, across the entire range of $0 < d \leqslant R_S$ and for different λ_p (recall $\lambda_p = n/(\pi R_C^2)$).

4.2 Modeling Transmission Success for Full-duplex

In the case of full-duplex networks, a pair of nodes X_i and Y_i that are selected for transmission can successfully exchange packets between its nodes only if $SIR_{X_i} > \beta$ and $SIR_{Y_i} > \beta$, where SIR_{X_i} is the SIR considered at the primary transmitter X_i for its reception from the secondary transmitter Y_i, and

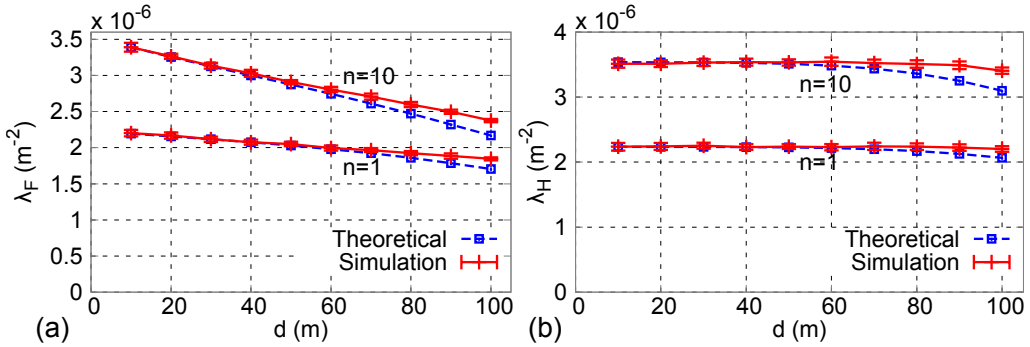

Figure 4.1: Density of Successful Transmissions vs. link distance of (a) Half-duplex CSMA networks (b) Full-duplex CSMA networks under physical model.

$$SIR_{X_i} := \frac{P h_{Y_i X_i} d^{-\alpha}}{\sum_{(X_j,Y_j)\in\Phi^F_m, j\neq i} P h_{X_j X_i} \|X_j - X_i\|^{-\alpha} + P h_{Y_j X_i} \|Y_j - X_i\|^{-\alpha}} > \beta.$$

The SIR at the secondary transmitter Y_i can be defined similarly. The channel fading coefficients follow the same model as in the half-duplex case. Note however that the interference term is attributed to not only other primary transmitters X_j, but also the associated secondary transmitters Y_j.

Consider a given full-duplex pair q_i. Assuming a symmetric channel between the primary and secondary transmitter, we have $h_{X_i Y_i} = h_{Y_i X_i} = h_i$. Also, as the magnitude of received signal power at a node is dominated by *path-loss*, we assume that the channel fading coefficients between different nodes of two pairs q_i and q_j are the same i.e. $h_{X_j X_i} = h_{X_j Y_i} = h_{Y_j X_i} = h_{Y_j Y_i}$. We denote the representative channel fading coefficient from pair q_j to pair q_i by h^i_j. So, we are left with one set of *i.i.d* representative channel fading coefficients $\{h^i_j\}$ between different pairs i and j. A successful transmission thus needs to satisfy the following conditions for SIR_{X_i} and SIR_{Y_i}:

$$SIR_{X_i} := \frac{h_i d^{-\alpha}}{\sum_{q_j\in\Phi^F_m, j\neq i} h^i_j \left(\|X_j - X_i\|^{-\alpha} + \|Y_j - X_i\|^{-\alpha}\right)} > \beta$$

$$SIR_{Y_i} := \frac{h_i d^{-\alpha}}{\sum_{q_j\in\Phi^F_m, j\neq i} h^i_j \left(\|X_j - Y_i\|^{-\alpha} + \|Y_j - Y_i\|^{-\alpha}\right)} > \beta$$

The probability that two nodes in a typical full-duplex pair (X_o, Y_o) successfully transmit to each other is then given by $\mathbb{P}^{!o}_{\Phi^F_m}(SIR_{X_o} > \beta, SIR_{Y_o} > \beta)$, which we derive as follows.

Theorem 4.2. *Under the physical model, the successful transmission probability for a typical full-duplex bi-directional link can be approximated by:*

$$\mathbb{P}^{!o}_{\Phi^F_m}(SIR_{X_o} > \beta,\ SIR_{Y_o} > \beta) \approx$$

$$\frac{1}{2\pi}\int_0^{2\pi} exp\left\{-\frac{\lambda_p^2}{2\pi\lambda_m^f}\int_0^{\infty}\int_0^{2\pi}\int_0^{2\pi} k(r,\theta,\phi,\delta)\ \Delta(r,\theta,\phi,\delta) r dr d\theta d\delta\right\} d\phi$$

where, $k(r,\theta,\phi,\delta)$ denotes the probability that two pairs q_i and q_j of $\tilde{\Phi}_o$ are retained in Φ^F_m and is given by,

$$k(r,\theta,\phi,\delta) = \begin{cases} 0, & (r,\theta,\phi,\delta) \in B_1 \cup B_2 \cup B_3 \cup B_4 \\ 2g(V_1), & \text{otherwise} \end{cases}$$

$$\text{and, } g(V_1) = \frac{V_1(1-e^{-\lambda_p V_F}) - V_F(1-e^{-\lambda_p V_1})}{\lambda_p^2 V_F V_1 (V_1 - V_F)}$$

where V_F follows Theorem 3.4, and λ^f_m equals λ_F (Eq. 3.9). V_1, B_1 to B_4 and $\Delta(r,\theta,\phi,\delta)$ are parameters detailed in Appendix A.5.

Proof: Available in Appendix A.5. □

In Fig. 4.1 (b) we compare the simulation results for the density of successful transmissions of full-duplex CSMA networks and the above approximation. We simulate 20 topologies and observe that the estimation obtained is in close agreement with the simulation results across different d and λ_p settings.

4.3 Full-duplex Gain under Physical Model

Under the physical model, the spatial network throughput can be calculated as the product of the intensity of concurrent transmissions and

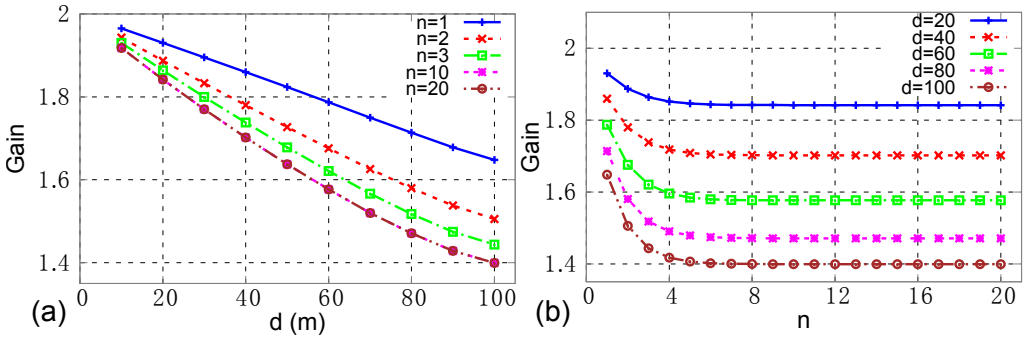

Figure 4.2: Full-duplex gain under the physical model.

the probability that a transmission is successful. The throughput for the half-duplex CSMA networks, denoted as T_H, is thus given by,

$$T_H = \lambda_m^h \, \mathbb{P}^{!o}_{\Phi_m^H}(SIR_{Y_o} > \beta)$$

where λ_m^h is given by Eq. (4.1) and $\mathbb{P}^{!o}_{\Phi_m^H}(SIR_{Y_o} > \beta)$ can be obtained from the result in Theorem 4.1.

For the full-duplex CSMA networks, the network throughput can be derived as,

$$T_F = 2\lambda_m^f \, \mathbb{P}^{!o}_{\Phi_m^F}(SIR_{X_o} > \beta, \; SIR_{Y_o} > \beta)$$

where λ_m^f is given by Eq. (3.9) and $\mathbb{P}^{!o}_{\Phi_m^F}(SIR_{X_o} > \beta, \; SIR_{Y_o} > \beta)$ can be obtained following Theorem 4.2. There is multiplication by a factor 2 because λ_m^f is the density of transmission pairs and every pair has two active transmissions.

In Fig. 4.2 we plot the network throughput gain of full-duplex over half-duplex CSMA networks, T_F/T_H, with varying link distance d and deployment density λ_p where $\lambda_p = n/\pi R_C^2$. *We observe that the full-duplex gain shows similar trend as in the protocol model*, *i.e.*, it approaches 2 as d is near 0, but decreases to around 1.4 as d approaches R_S.

We also observed that the carrier sensing range R_C is a crucial parameter that affects the spatial throughput. Fig. 4.3(a) plots the numerical

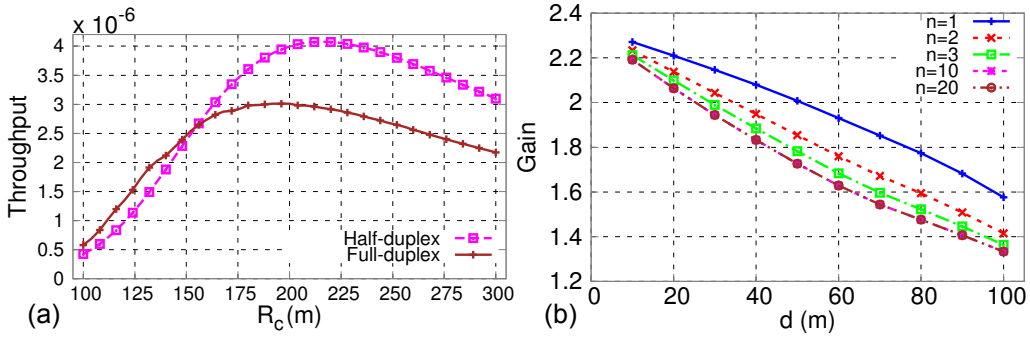

Figure 4.3: (a) Spatial throughput vs. carrier sensing range. Optimal $R_C = 200$m for full-duplex and $R_C = 216$m for half-duplex (b) Gain of full-duplex over half-duplex CSMA networks under physical model using the optimal R_C.

spatial throughput under different R_C settings, with SIR threshold $\beta = 10$ dB, $\alpha = 4$ and maximum link distance 100m. A smaller R_C may not be able to protect the receiver from interference, whereas a larger R_C degrades spatial reuse between links. Remarkably, *the throughput-optimal* R_C *for full-duplex is smaller than that of half-duplex*, again because of full-duplex's capability of perfect carrier sensing. Each full-duplex receiver itself is a transmitter, and hence it does not require the other transmitter to extend R_C to protect it. From Fig. 4.3 (b) we can see that under the optimal R_C values the full-duplex can provide a throughput gain larger than 2 for smaller link distances (*e.g.*, 2.3$\times$ for $d = 10$m). This is another aspect that network planners need to consider to capitalize on full-duplex technology. Given the consistency of physical and protocol model, we expect a varying R_C will affect the full-duplex gain in the protocol model as well. We leave the detailed exploration for future work.

— 5 —

Application to Full-duplex Network Planning

In this section, we extend our analytical results to derive guidelines for deploying full-duplex multi-cell wireless networks. For network planners, an important consideration is to balance achievable throughput with deployment cost. This can be reflected in a throughput-per-cost metric, denoted as η. So, given an anticipated coverage area, one approach to network planning would be to compare the η of full- and half-duplex AP deployment, and choose the one that is more profitable.

But before the deployment, it is necessary to ensure that the AP density is sufficient to cover the region of interest. The fraction f_A, of an area A, covered by a homogeneous PPP deployment with density λ is given by: $f_A = 1 - e^{-\lambda\pi R_C^2}$, where R_C represents the carrier sensing range of an AP [22]. Thus, the deployment density should satisfy:

$$\lambda \geqslant \lambda_0 = -\ln(1 - f_A)/\pi R_C^2 \tag{5.1}$$

For a given client population, suppose each client associates to the nearest AP. For an arbitrarily located client, its mean distance to the nearest AP can be modeled by [22]: $d = (2\sqrt{\lambda})^{-1}$.

Naturally, as the APs' deployment density λ increases, the mean AP-client link distance decreases.

Let λ_H and λ_F denote the density of successful transmissions (in m^{-2}) for half- and full-duplex deployment. Taking the protocol model in Sec. 3 for example, we can express λ_F and all three cases of λ_H as a function of d, R_C and λ. Suppose the cost of a half-duplex and full-duplex AP equals c_H and c_F, and throughput-per-cost equals η_H and η_F, respectively. For a per-link (one-direction) bit-rate b Mbps, we have:

$$\eta_H = \frac{\lambda_H A b}{\lambda A c_H}, \text{ and } \eta_F = \frac{2\lambda_F A b}{\lambda A c_F} \tag{5.2}$$

Given that $d = (2\sqrt{\lambda})^{-1}$, the η_H (η_F) can be expressed as a function of λ, R_C, b and A. In practice, the latter three parameters are known, and thus η_H (η_F) is only a function of λ, which can be straightforwardly proven to be *monotonically decreasing* using the closed-form formulas in Sec. 3. Consider the following set of practical parameters: $c_H = 50\$$, $c_F = Kc_H$; $A = 9e4$ m^2, $R_C = 100m$, $b = 6$ Mbps, and $f_A = 90\%$ which can be fed into Eq. (5.2). We depict the results in Fig. 5.1(a) , considering only the practical cases of imperfect carrier sensing and RTS/CTS for λ_H. We observe that η is high for a sparse network, but decreases fast as network density increases The rate of decrease drops as the network becomes denser, primarily because of the saturation of spatial throughput. η_H can outperform η_F only for large K values.

This inspires us to examine the sweet-spot K value, K_t, below which a full-duplex deployment becomes more cost-effective. Observing η_H and η_F are monotonic, we can set $\eta_H = \eta_F$, and based on Eq. (5.2), solve for K_t:

$$K_t = c_F/c_H = 2\lambda_F/\lambda_H \tag{5.3}$$

which in turn becomes a function of λ. With the aforementioned configurations, numerical results in Fig. 5.1(b) show that K_t sits above 1.8 and increases monotonically with deployment density. With the above

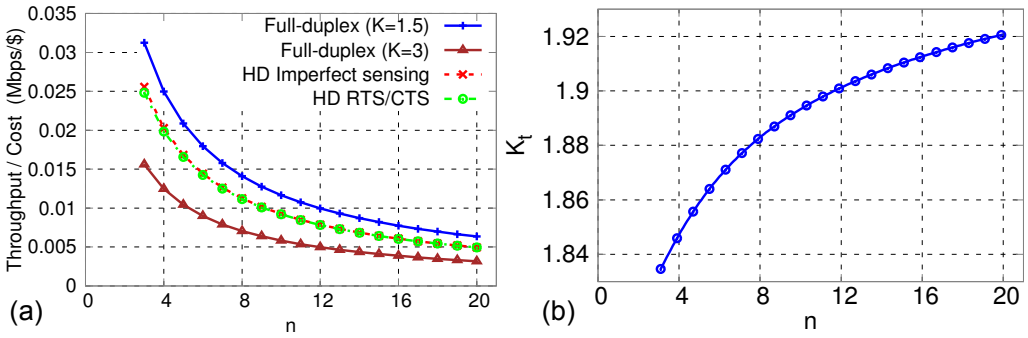

Figure 5.1: (a) Throughput/Cost vs. network density for different K, and (b) The trade-off point K_t under different AP densities.

analytical framework, network planners can easily obtain the sweet spot and decide the optimal choice.

— 6 —

Related Work

Recent research on full-duplex mainly focuses on implementing new radio hardware architecture and signal processing algorithms. Choi *et al.* [9] is the first to realize single-channel full-duplex over ZigBee radios, which inspired substantial follow-on efforts. In particular, Bharadia *et al.* [10] recently implemented the first in-band full-duplex WiFi radio with a single antenna.

The development of full-duplex radios is marching steadily towards commercialization [7]. In contrast, the impact of full-duplex on higher network layers remains largely underexplored. Centralized scheduling and decentralized random access protocols [12, 11] have been proposed for full-duplex wireless LANs. Each of these protocols modifies the current CSMA MAC to capitalize on the concurrent transmission/reception capability. The performance limit of full-duplex and its dominating factors are yet to be investigated.

Since the landmark paper of Gupta and Kumar [13], substantial effort has focused on analyzing wireless network capacity under various topologies and PHY layer technologies [26]. Existing analysis mostly assumes half-duplex radios, and targets capacity scaling laws under an asymptotically growing node population. Information theoretic properties of single-cell full-duplex WLAN are analyzed recently [27]. Yet it remains an

open problem what is the fundamental gain when full-duplex interplays with multi-cell interference and spatial reuse.

Recent work of Yang *et al.* [28] used a simplified unit-disk model to compare the asymptotic dominance relation (higher or lower) between MIMO and full-duplex radio modes. Xie *et al.* [14] are the first to derive an upperbound of full-duplex network capacity through disk-packing. In contrast, our approach leverages stochastic geometry for an *average-case analysis* of the full-duplex capacity and its gain over half-duplex. Our analysis shows consistent trend with [14], *i.e.*, the gain decreases as link distance approaches interference range. However, our framework can analyze the impact of a more comprehensive set of network parameters, carrier sensing models, and interference model.

Stochastic geometry has shown great potential in quantifying the spatial reuse in wireless networks [15]. Particularly to IEEE 802.11 networks, the key analytic question lies in approximating the *sparsified* winning node distribution after contention [21]. In [8], an HCPP model is proposed to capture key properties of 802.11 networks (for Poisson node distribution). Alfano *et al.* [29] extended model to analyze the nodes' throughput variation under a minimum link-distance constraint. Substantial work has focused on more accurate approximation of contention behavior [21]. To our knowledge, our analytical framework is the first to advance stochastic geometry to analyze full-duplex wireless networks. Our analysis overcomes the limitations of classical stochastic geometry (Sec. 1), and enables an investigation of different carrier sensing schemes for both full- and half-duplex networks.

— 7 —

Conclusion

We have devised a spatial stochastic framework, which is tailored to analyzing the spatial footprint of full-duplex and half-duplex links under perfect/imperfect carrier sensing and RTS/CTS signaling. Our framework introduces a new analytic tool, *i.e.*, the mean contention region, that integrates classical stochastic geometry with the protocol interference model. This allows us to establish closed-form formulas for the full-duplex gain under different topological properties and protocol imperfectness. Our analysis under the physical model, though consistent with the protocol model, builds on probabilistic approximations. Our immediate next step is to derive a more accurate and concise model along this line of analysis.

— A —

Appendix

A.1 Proof of Theorem 3.3 (See page 18)

The expressions in Theorem 3.3 are given by:

$$\gamma_1 = \arccos\left(\frac{R_I^2 + d^2 - R_S^2}{2dR_I}\right) \qquad \gamma_2 = \arccos\left(\frac{R_S^2 + d^2 - R_I^2}{2dR_S}\right)$$

$$\theta_1 = \arccos\left(\frac{d^2 + r^2 - R_I^2}{2dr}\right) \qquad \theta_2 = \arccos\left(\frac{r^2 + R_I^2 - d^2}{2rR_I}\right)$$

$$\theta_3 = \arccos\left(\frac{r^2 + R_S^2 - d^2}{2rR_S}\right) \qquad \theta_4 = \arccos\left(\frac{d^2 + r^2 - R_S^2}{2dr}\right)$$

$$\theta_5 = \arccos\left(\frac{r}{2R_S}\right) \qquad \theta_6 = \arccos\left(\frac{r}{2R_I}\right)$$

$$\varphi_1 = \arccos\left(\frac{{\delta_1}^2 + d^2 - R_I^2}{2d\delta_1}\right) \qquad \varphi_2 = \arccos\left(\frac{{\delta_1}^2 + {\delta_2}^2 - d^2}{2\delta_1\delta_2}\right)$$

$$\varphi_3 = \arccos\left(\frac{{\delta_2}^2 + d^2 - R_S^2}{2d\delta_2}\right) \qquad \varphi_4 = \arccos\left(\frac{2r^2 + 2dr\cos(\theta)}{2r\sqrt{d^2 + r^2 + 2dr\cos(\theta)}}\right)$$

$$\varphi_5 = \arccos\left(\frac{2d^2 + r^2 + 2dr\cos(\theta) - R_I^2}{2d\sqrt{d^2 + r^2 + 2dr\cos(\theta)}}\right)$$

$$\delta_1 = \sqrt{r^2 + R_I^2 + 2rR_I\cos(\theta - \gamma_1)} \qquad \delta_2 = \sqrt{r^2 + R_S^2 - 2rR_S\cos(\theta + \gamma_2)}$$

The proof follows similar steps as the full-duplex case below, and is thus omitted to avoid redundancy. □

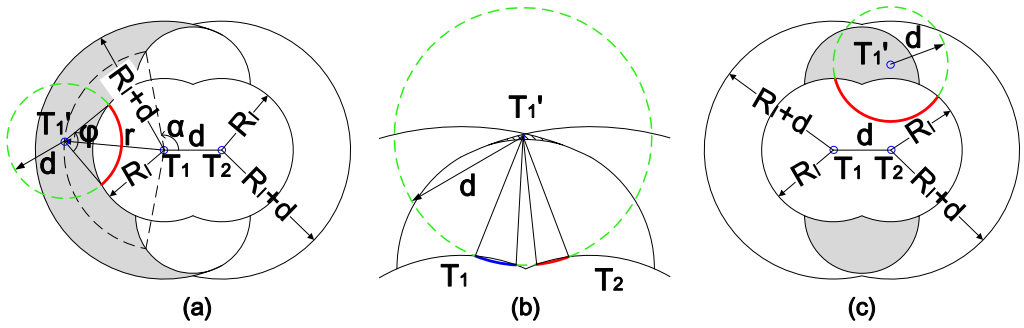

Figure A.1: (a) The left-hand side area in second situation, (b) the overlaying area of left-hand side area and right-hand side area, (c) the area in third situation.

A.2 Proof of Theorem 3.4 (See page 19)

Proof: We consider three regions shown as different patterns in Fig. 3.2(c) around typical link $\mathcal{L}_o$.

First, the union of primary transmitter T_1's and secondary transmitter T_2's interference range (V_1), which is blank region, should be counted as a deterministic contention region.

Second, consider a contending link $\mathcal{L}'$ whose primary transmitter $T_1^{'}$ exists within the grey area in Fig. A.1(a), then its associated secondary transmitter $T_2^{'}$ may be located within T_1's interference range, which leads to contention with $\mathcal{L}_o$. The derivation of this spatial averaged contention region (V_2) is similar to Theorem 3.1. The symmetric region on the RHS in the same figure can be calculated in the same way.

There is a small area (shaded area in Fig. A.1(b)) that needs special consideration: if another primary transmitter $T_1^{'}$ resides there, its secondary transmitter $T_2^{'}$ could fall in T_1 or T_2's interference range. For the LHS, we only need to consider $T_2^{'}$ is located within T_1's interference range; and similarly RHS for T_2's interference range.

Third, consider a contending link $\mathcal{L}'$ with its transmitter lying in the upper shaded area in Fig. A.1(c). The associated secondary transmitter

$T_2^{'}$ can reside in both primary transmitter T_1 and secondary transmitter T_2's interference range. This is different from situation 2 as the potential location of $T_2^{'}$ is continuous, which corresponds to V_3.

Finally, any area outside the above cases falls outside the potential contention region of the typical full-duplex link. □

A.3 Proof of Proposition 1 (See page 29)

Proof: From Fig. 3.1(d), the condition for successful bi-directional full-duplex transmission is that the shaded region cannot be reused by other T_1/T_2, and we can obtain MCR for it as V_F(Theorem 3.4). Based on Fig. 3.8 we elucidate the spatial occupation of cut-through transmission. Observing both the transmitter and secondary receiver operate in half-duplex mode. So we consider two situations here.

First, considering the case of perfect carrier sensing, the condition for successful transmission as shown in Fig. 3.8(a) is the blue hatched region cannot be reused by any other T/R_1, grey shaded region cannot be reused by any other R_1/R_2 and the blank region cannot be reused any other $T/R_1/R_2$. If we assume that the blank region can be reused by other R_2 then the MCR of $R_1 \leftrightarrow R_2$ link is equivalent to that of a bi-directional link (V_F). In fact, if we restrict other R_2 from being present in the blank region, then the above MCR would be larger than V_F. Furthermore, as MCR for the grey region is nonzero, the total MCR for cut-through transmission with perfect carrier sensing is larger than that of a bi-directional link.

Second, for imperfect carrier sensing case, the successful transmission condition should be no other $T/R_1/R_2$ in the grey region and no other T/R_1 in the blue hatched region. Suppose that the grey region can be reused by other R_2. Then, the MCR of $T \leftrightarrow R_1$ link is equivalent to that of a bi-directional link. Actually, if allow other R_2 in the grey region then the above MCR would be larger than V_F. Furthermore, as the MCR for blue

hatched region is nonzero, the total MCR for cut-through transmission with imperfect carrier sensing is larger than that of a bi-directional link as well.

We conclude that in either case the spatial occupation for cut-through transmission is always larger than that of bi-directional transmission, and therefore its network throughput is lower. □

A.4 Proof of Theorem 4.1 (See page 32)

Proof: We first calculate the probability of SIR coverage at the receiver conditioned on its orientation ϕ with the horizontal i.e. we first calculate $\mathbb{P}^{!o}_{\Phi^H_m}(SIR_{Y_o} > \beta \mid \phi)$. Then, in the end we get $\mathbb{P}^{!o}_{\Phi^H_m}(SIR_{Y_o} > \beta)$ by deconditioning on ϕ. To reduce notational complexity, in this proof we will henceforth refer to probability of coverage conditioned on ϕ as $\mathbb{P}^{!o,\phi}_{\Phi^H_m}(SIR_{Y_o} > \beta)$.

$$
\begin{aligned}
&\mathbb{P}^{!o,\phi}_{\Phi^H_m}(SIR_{Y_o} > \beta) \\
&= \mathbb{P}^{!o,\phi}_{\Phi^H_m}\left(\frac{P h_{X_o Y_o} d^{-\alpha}}{\sum_{X_j \in \Phi^H_m} P h_{X_j Y_o} \|X_j - Y_o\|^{-\alpha}} > \beta \right) \\
&= \mathbb{P}^{!o,\phi}_{\Phi^H_m}\left(h_{X_o Y_o} > \beta d^{\alpha} \sum_{X_j \in \Phi^H_m} h_{X_j Y_o} \|X_j - Y_o\|^{-\alpha} \right) \\
&= \mathbb{E}^{!o,\phi}_{\Phi^H_m, h_{X_j Y_o}}\left[\exp\left\{ -\beta d^{\alpha} \sum_{X_j \in \Phi^H_m} h_{X_j Y_o} \|X_j - Y_o\|^{-\alpha} \right\} \right] \qquad \text{(A.1)} \\
&= \mathbb{E}^{!o,\phi}_{\Phi^H_m}\left[\mathbb{E}_{h_{X_j Y_o}}\left[\prod_{X_j \in \Phi^H_m} \exp\left\{ -\beta d^{\alpha} h_{X_j Y_o} \|X_j - Y_o\|^{-\alpha} \right\} \right] \right] \\
&= \mathbb{E}^{!o,\phi}_{\Phi^H_m}\left[\prod_{X_j \in \Phi^H_m} \mathbb{E}_{h_{X_j Y_o}}\left[\exp\left\{ -\beta d^{\alpha} h_{X_j Y_o} \|X_j - Y_o\|^{-\alpha} \right\} \right] \right] \qquad \text{(A.2)} \\
&= \mathbb{E}^{!o,\phi}_{\Phi^H_m}\left[\prod_{X_j \in \Phi^H_m} \frac{1}{1 + \beta \left(\frac{d}{\|X_j - Y_o\|} \right)^{\alpha}} \right]
\end{aligned}
$$

$$= \mathbb{E}^{!o,\phi}_{\Phi^H_m}\left[exp\left\{ - \sum_{X_j \in \Phi^H_m} \ln\left(1 + \beta\left(\frac{d}{\|X_j - Y_o\|}\right)^{\alpha}\right)\right\}\right]$$

$$> exp\left\{ -\mathbb{E}^{!o,\phi}_{\Phi^H_m}\left[\sum_{X_j \in \Phi^H_m} \ln\left(1 + \beta\left(\frac{d}{\|X_j - Y_o\|}\right)^{\alpha}\right)\right]\right\} \tag{A.3}$$

$$= exp\left\{ -\mathbb{E}^{!o,\phi}_{\Phi^H_m}\left[\sum_{(r,\theta)\in\Phi^H_m} \Delta(r,\theta,\phi)\right]\right\}$$

$$= exp\left\{ -\frac{1}{\lambda^h_m}\int_0^{\infty}\int_0^{2\pi} \rho^{(2)}(r,\theta)\Delta(r,\theta,\phi) r dr d\theta\right\} \tag{A.4}$$

$$= exp\left\{ -\frac{\lambda^2_p}{\lambda^h_m}\int_0^{\infty}\int_0^{2\pi} k(r,\theta)\Delta(r,\theta,\phi) r dr d\theta\right\} \tag{A.5}$$

To get Eq. (A.1) we condition on the point process Φ^H_m and $h_{X_j Y_o}$ and use the fact that $h_{X_o Y_o}$ is an exponential random variable with $\mathbb{E}(h_{X_o Y_o}) = 1$. As $\{h_{X_j Y_o}\}$ are a set of *i.i.d* random variables, we get Eq. (A.2). To get Eq. (A.3) we apply *Jensen's* inequality using the fact that $exp(-.)$ is a strictly convex function. We get Eq. (A.4) by applying *Campbell's* theorem [23] to the previous step. To get Eq. (A.5) we use the relation between *second-order product density* of the stationary point process Φ^H_m and $k(r,\theta)$ based on [30]. Finally, by deconditioning Eq. (A.5) *w.r.t* ϕ, we can get the statement of Theorem 4.1. □

A.5 Proof of Theorem 4.2 (See page 34)

Proof: We first introduce the following quantities. Consider the two full-duplex pairs q_i and q_j shown in Fig. A.2. We define,
(a) B_1 to be the set of (r,θ,ϕ,δ) values such that X_j and X_i are within R_C of each other. We similarly define B_2, B_3, B_4 for the cases when X_j and Y_i are within R_C of each other, Y_j and X_i are within R_C of each other, and Y_j and Y_i are within R_C of each other, respectively. Thus we have,

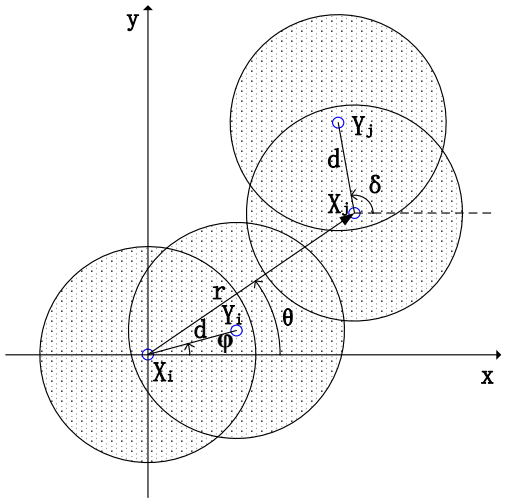

Figure A.2: Illustration of two full-duplex pairs

$$
\begin{aligned}
B_1 &= \{(r,\theta,\phi,\delta) : r \leqslant R_C\},\\
B_2 &= \{(r,\theta,\phi,\delta) : r^2 + d^2 - 2rd\cos(\theta-\phi) \leqslant R_C^2\},\\
B_3 &= \{(r,\theta,\phi,\delta) : r^2 + d^2 + 2rd\cos(\theta-\delta) \leqslant R_C^2\},\\
B_4 &= \{(r,\theta,\phi,\delta) : [(r\cos\theta + d\cos\delta) - d\cos\phi]^2 +\\
&\qquad [(r\sin\theta + d\sin\delta) - d\sin\phi]^2 \leqslant R_C^2\}
\end{aligned}
$$

(b) $V_1(r,\theta,\phi,\delta)$ is the mean contention region around two pairs q_i and q_j that are contending with other full-duplex links.

(c) $\Delta(r,\theta,\phi,\delta) =$

$$
\begin{aligned}
&\ln\left(1 + \frac{\beta}{2} d^{\alpha}\Big\{ r^{-\alpha} + \Big(r^2 + d^2 + 2rd\cos(\theta-\delta)\Big)^{-\frac{\alpha}{2}}\right.\\
&+ \Big(r^2 + d^2 - 2rd\cos(\theta-\phi)\Big)^{-\frac{\alpha}{2}} + (\ [(r\cos\theta + d\cos\delta) - d\cos\phi]^2\\
&\left. + [(r\sin\theta + d\sin\delta) - d\sin\phi]^2\ )^{-\frac{\alpha}{2}} \Big\}\right)
\end{aligned}
$$

The probability that two nodes in a pair successfully transmit to each other, $\mathbb{P}^{!o}_{\Phi_m^F}(SIR_{X_o} > \beta, SIR_{Y_o} > \beta)$ can be upper bounded by,

$$\mathbb{P}^{!o}_{\Phi^F_m}\Bigg(h_o > \frac{\beta}{2} d^\alpha \sum_{q_j \in \Phi^F_m} h^o_j \{ \|X_j - X_o\|^{-\alpha} + \|Y_j - X_o\|^{-\alpha} + \|X_j - Y_o\|^{-\alpha} + \|Y_j - Y_o\|^{-\alpha} \}\Bigg) \tag{A.6}$$

Later in the proof, we get a lower bound on (A.6) using *Jensen's* inequality which serves as an estimate of $\mathbb{P}^{!o}_{\Phi^F_m}(SIR_{X_o} > \beta, SIR_{Y_o} > \beta)$. We validate this estimate by comparing it to the simulation results. We first obtain (A.6) by conditioning it the orientation ϕ of the secondary transmitter of the typical pair. To reduce notational complexity, we will denote this conditioning in the Reduced Palm measure as $\mathbb{P}^{!o,\phi}_{\Phi^F_m}$. Then, in the end we obtain the estimate by deconditioning *w.r.t* ϕ. Also, in the following lines of the proof we will denote the term $\{\|X_j - X_o\|^{-\alpha} + \|Y_j - X_o\|^{-\alpha} + \|X_j - Y_o\|^{-\alpha} + \|Y_j - Y_o\|^{-\alpha}\}$ in (A.6) by l^o_j. Thus we have,

$$\mathbb{P}^{!o,\phi}_{\Phi^F_m}\left(h_o > \frac{\beta}{2} d^\alpha \sum_{q_j \in \Phi^F_m} h^o_j l^o_j\right)$$

$$= \mathbb{E}^{!o,\phi}_{\Phi^F_m, h^o_j}\left[exp\left\{-\frac{\beta}{2} d^\alpha \sum_{q_j \in \Phi^F_m} h^o_j l^o_j\right\}\right] \tag{A.7}$$

$$= \mathbb{E}^{!o,\phi}_{\Phi^F_m}\left[\mathbb{E}_{h^o_j}\left[\prod_{q_j \in \Phi^F_m} exp\left\{-\frac{\beta}{2} d^\alpha h^o_j l^o_j\right\}\right]\right]$$

$$= \mathbb{E}^{!o,\phi}_{\Phi^F_m}\left[\prod_{q_j \in \Phi^F_m} \mathbb{E}_{h^o_j}\left[exp\left\{-\frac{\beta}{2} d^\alpha h^o_j l^o_j\right\}\right]\right] \tag{A.8}$$

$$= \mathbb{E}^{!o,\phi}_{\Phi^F_m}\left[\prod_{q_j \in \Phi^F_m} \frac{1}{1 + \frac{\beta}{2} d^\alpha l^o_j}\right]$$

$$= \mathbb{E}^{!o,\phi}_{\Phi^F_m}\left[exp\left\{-\sum_{q_j \in \Phi^F_m} \ln\left(1 + \frac{\beta}{2} d^\alpha l^o_j\right)\right\}\right]$$

$$> exp\left\{-\mathbb{E}^{!o,\phi}_{\Phi^F_m}\left[\sum_{q_j\in\Phi^F_m}\ln\left(1+\frac{\beta}{2}d^{\alpha}l^o_j\right)\right]\right\} \tag{A.9}$$

$$= exp\left\{-\mathbb{E}^{!o,\phi}_{\Phi^F_m}\left[\sum_{q_j\in\Phi^F_m}\ln\left(1+\frac{\beta}{2}d^{\alpha}\left(\|X_j-X_o\|^{-\alpha}+\right.\right.\right.\right.$$

$$\left.\left.\left.\left.\|Y_j-X_o\|^{-\alpha}+\|X_j-Y_o\|^{-\alpha}+\|Y_j-Y_o\|^{-\alpha}\right)\right)\right]\right\} \tag{A.10}$$

$$= exp\left\{-\mathbb{E}^{!o,\phi}_{\Phi^F_m}\left[\sum_{(r,\theta,\delta)\in\Phi^F_m}\Delta(r,\theta,\phi,\delta)\right]\right\}$$

$$= exp\left\{-\frac{1}{\lambda^f_m}\int_0^{\infty}\int_0^{2\pi}\int_0^{2\pi}\rho^{(2)}(r,\theta,\phi,\delta)\Delta(r,\theta,\phi,\delta)rdrd\theta d\delta\right\} \tag{A.11}$$

$$= exp\left\{-\frac{\lambda^2_p}{2\pi\lambda^f_m}\int_0^{\infty}\int_0^{2\pi}\int_0^{2\pi}k(r,\theta,\phi,\delta)\Delta(r,\theta,\phi,\delta)rdrd\theta d\delta\right\} \tag{A.12}$$

To get Eq.(A.7) we condition on the point process Φ^F_m and h^o_j and use the fact that h_o is an exponential random variable with $\mathbb{E}(h_o) = 1$. As $\{h^o_j\}$ are a set of *i.i.d* random variables, we get Eq.(A.8). To get Eq.(A.9) we apply *Jensen's* inequality using the fact that $exp(-.)$ is a strictly convex function. We get Eq.(A.10) by just replacing l^o_j with term of (A.6) mentioned previously. We get Eq.(A.11) by applying *Campbell's* theorem [23] to the previous step. To get Eq.(A.12) we use the relation between *second-order product density* of the stationary point process Φ^F_m and $k(r,\theta,\phi,\delta)$ based on [30]. Finally, by deconditioning Eq.(A.12) *w.r.t* ϕ, we get a lower bound on (A.6) which is the estimate mentioned in the statement of Theorem 4.2 . We note that the function $g(V_1)$ can be obtained in an analogous manner to the derivation of the function $\eta(V)$ given in the analysis of mean interference for *Matern* type II process in *Zhong et al.* [16]. □

Bibliography

[1] E. N. Gilbert, "Random plane networks," *Journal of the Society for Industrial & Applied Mathematics*, vol. 9, no. 4, pp. 533–543, 1961.

[2] H. ElSawy, E. Hossain, and S. Camorlinga, "Characterizing random csma wireless networks: A stochastic geometry approach," in *Communications (ICC), 2012 IEEE International Conference on*. IEEE, 2012, pp. 5000–5004.

[3] B. Blaszczyszyn and P. Muhlethaler, "Stochastic analysis of non-slotted aloha in wireless ad-hoc networks," in *INFOCOM, 2010 Proceedings IEEE*. IEEE, 2010, pp. 1–9.

[4] L. Kleinrock and J. Silvester, "Optimum transmission radii for packet radio networks or why six is a magic number," in *NTC'78; National Telecommunications Conference, Volume 1*, vol. 1, 1978, p. 4.

[5] Cisco, "Cisco Visual Networking Index: Forecast and Methodology, 2013âŁ"2018," 2015.

[6] M. Jain, J. I. Choi, T. Kim, D. Bharadia, S. Seth, K. Srinivasan, P. Levis, S. Katti, and P. Sinha, "Practical, Real-time, Full Duplex Wireless," in *Proc. of ACM MobiCom*, 2011.

[7] Kumu Networks, "Wireless Full-duplex: A Revolution in Wireless Design," http://kumunetworks.com/, 2014.

[8] H. Q. Nguyen, F. Baccelli, and D. Kofman, "A Stochastic Geometry Analysis of Dense IEEE 802.11 Networks," in *IEEE INFOCOM*, 2007.

[9] J. I. Choi, M. Jain, K. Srinivasan, P. Levis, and S. Katti, "Achieving Single Channel, Full Duplex Wireless Communication," in *ACM MobiCom*, 2010.

[10] D. Bharadia, E. McMilin, and S. Katti, "Full Duplex Radios," in *Proceedings of ACM SIGCOMM*, 2013.

[11] W. Zhou, K. Srinivasan, and P. Sinha, "RCTC: Rapid Concurrent Transmission Coordination in Full Duplex Wireless Networks," in *Proc. of IEEE ICNP*, 2013.

[12] A. Sahai, G. Patel, and A. Sabharwal, "Pushing the Limits of Full-duplex: Design and Real-time Implementation," *CoRR*, vol. abs/1107.0607, 2011.

[13] P. Gupta and P. Kumar, "The Capacity of Wireless Networks," *IEEE Transactions on Information Theory*, vol. 46, no. 2, 2000.

[14] X. Xie and X. Zhang, "Does Full-duplex Double the Capacity of Full-Duplex Wireless Networks?" in *Proc. of IEEE INFOCOM*, 2014.

[15] J. Andrews, R. Ganti, M. Haenggi, N. Jindal, and S. Weber, "A Primer on Spatial Modeling and Analysis in Wireless Networks," *IEEE Comm. Magazine*, vol. 48, no. 11, 2010.

[16] Y. Zhong, W. Zhang, and M. Haenggi, "Stochastic Analysis of the Mean Interference for the RTS/CTS Mechanism," in *IEEE ICC*, 2014.

[17] F. Baccelli, B. Blaszczyszyn, and P. Muhlethaler, "Stochastic Analysis of Spatial and Opportunistic Aloha," *IEEE JSAC*, vol. 27, no. 7, 2009.

[18] S. Gollakota and D. Katabi, "Zigzag Decoding: Combating Hidden Terminals in Wireless Networks," in *Proc. of ACM SIGCOMM*, 2008.

[19] M. Vutukuru, K. Jamieson, and H. Balakrishnan, "Harnessing Exposed Terminals in Wireless Networks," in *Proc. of USENIX NSDI*, 2008.

[20] X. Xie and X. Zhang, "Semi-Synchronous Channel Access for Full-duplex Wireless Networks," in *Proc. of IEEE ICNP*, 2014.

[21] A. Busson and G. Chelius, "Point Processes for Interference Modeling in CSMA/CA Ad-hoc Networks," in *Proc. of ACM PE-WASUN*, 2009.

[22] S. N. Chiu, D. Stoyan, W. S. Kendall, and J. Mecke, *Stochastic Geometry and Its Applications*. John Wiley & Sons, 2013.

[23] A. M. Ibrahim, T. A. ElBatt, and A. El-Keyi, "Coverage Probability Analysis for Wireless Networks Using Repulsive Point Processes," *CoRR*, vol. abs/1309.3597, 2013.

[24] B. Matérn, "Spatial variation," *Lecture Notes in Statistics*, vol. 36, 1986.

[25] M. Haenggi, "Mean Interference in Hard-Core Wireless Networks," *IEEE Communications Letters*, vol. 15, no. 8, pp. 792–794, 2011.

[26] C. Jiang, Y. Shi, Y. Hou, W. Lou, S. Kompella, and S. Midkiff, "Toward Simple Criteria to Establish Capacity Scaling Laws for Wireless Networks," in *Proc. of IEEE INFOCOM*, 2012.

[27] V. Aggarwal, M. Duarte, A. Sabharwal, and N. Shankaranarayanan, "Full- or Half-duplex? A Capacity Analysis with Bounded Radio Resources," in *IEEE Information Theory Workshop (ITW)*, 2012.

[28] Y. Yang, B. Chen, K. Srinivasany, and N. B. Shroff, "Characterizing the Achievable Throughput in Wireless Networks with Two Active RF chains," in *Proc. of IEEE INFOCOM*, 2014.

[29] G. Alfano, M. Garetto, and E. Leonardi, "New Insights Into the Stochastic Geometry Analysis of Dense CSMA Networks," in *Proc. of IEEE INFOCOM*, 2011.

[30] D. Stoyan and H. Stoyan, "On One of Matern's Hard-Core Point Process Models," *MATHEMATISCHE NACHRICHTEN*, vol. 122, pp. 205–214, 1985.